Russian Chemical Reviews **72** (11) 913 – 937 (2003) © 2003 Russian Academy of Sciences and Turpion Ltd

DOI 10.1070/RC2003v072n11ABEH000829

The characteristics of fractal disperse systems

V I Roldughin

Contents

I.	Introduction	913
II.	Experimental studies of the properties of fractal aggregates	913
III.	Hydrodynamics of fractal aggregates and their dispersions	920
IV.	Optical properties of fractal aggregates	924
V.	Capillary phenomena in fractal systems	926
VI.	The fractal surface	928
VII.	Aerogels	930
VIII.	Conclusion	932

Abstract. Experimental methods of determination of the fractal dimensions of fractal aggregates are described. The results of studies on aggregation of colloidal particles in different regimes are discussed. Data on the hydrodynamics of colloid dispersions containing fractal aggregates and on the rheology of fractal gels are presented. Capillary phenomena in fractal systems as well as the structural and mechanical properties of aerogels and peculiar features of the optical properties of fractal aggregates are described. The bibliography includes 395 references.

I. Introduction

Disperse systems are of frequent occurrence in nature. The solid component of such systems represents aggregates of colloidal particles, which were among the first physicochemical objects described in the framework of fractal geometry approach. Currently, most studies on fractals are also carried out using fractal aggregates as examples. This is due to the fact that these objects can form a variety of structures, which can be identified with ease in model experiments. It was also found that fractal aggregation provides a way of simulation of many processes which at first glance have nothing to do with particle aggregation.

Fractal aggregates are constituents of a vast variety of systems. Their properties to a great extent predetermine the physicochemical characteristics of the entire systems. In this review the emphasis is placed on the physical properties of aggregates. We will discuss the experimental methods of determining the structure of aggregates and the laws of aggregation, which are based on these properties. Both widely used experimental methods and some promising original techniques for determination of the fractal dimension of aggregates are considered.

V I Roldughin Institute of Physical Chemistry, Russian Academy of Sciences, Leninsky prosp. 31, 119991 Moscow, Russian Federation. Fax (7-095) 952 53 08. Tel. (7-095) 955 46 47.
E-mail: roldugin@phyche.ac.ru

Received February 2003
Uspekhi Khimii **72** (11) 1027 – 1054 (2003); translated by A M Raevsky

In the review we will show how the fractal parameters † of surfaces and the properties of aerogels (systems comprised of aggregates of the primary particles) can be determined. The properties of aerogels thus implicitly reflect those of fractal aggregates. Of great importance for both aerogels and fractal surfaces are the capillary phenomena. On the one hand, they form the basis for some methods of determination of the fractal dimension of porous media. On the other hand, they affect the evolution of the structure of aerogels, especially at high temperatures.

A large part of the review is concerned with the hydrodynamic characteristics of fractal aggregates. Undoubtedly, these characteristics are of great practical value, because they are responsible for many properties of colloidal dispersions. A wide range of conditions suitable for studying the hydrodynamic behaviour of fractal aggregates is due to frequent occurrence of colloidal dispersions.

Recently, considerable progress has been achieved in studies of the optical properties of fractal aggregates. Researchers perceived that it is the fractal structure of aggregates that strongly affects the electromagnetic field distribution inside them. The fractal structure causes localisation of the electromagnetic field and a dramatic increase in its strength in some local domains. The effects revealed are of interest for all researchers who study highly dispersed metallic systems.

II. Experimental studies of the properties of fractal aggregates

1. Methods of determination of the fractal dimension

The most widely used methods of determination of the fractal dimension of aggregates include (i) sedimentation technique, (ii) electron and optical microscopy and (iii) light, X-ray and neutron scattering. The highest efficiency is provided by the third group of methods, while both microscopy techniques are most easy in use.

The methods based on optical and electron microscopy involve the determination of the dependence of the masses of aggregates on their sizes or construction of the plot of the density correlation function for an image of an aggregate.[2–6] They can be used to study the aggregates whose fractal dimension (d_f) is at

† For the definitions of the most important fractal parameters, see Ref. 1.

most two, because at $d_f > 2$ the images of a large proportion of the primary particles will overlap. Strictly speaking, some corrections [7] for the overlap of the particle images should be included even if one deals with fractal aggregates characterised by $d_f < 2$.

Two main approaches are employed in the microscopy studies. One of them involves plotting the density correlation function determined using the image of the aggregate *vs*. the distance from the centre of the aggregate in the double logarithmic coordinates. For fractal aggregates, the plot obtained must be linear. In this case, the fractal dimension can be determined from the slope of the plot using the known relationship for the density distribution function, $\rho(r)$, in the aggregate (see Ref. 1)

$$\rho(r) \propto r^{d_f - d}, \tag{1}$$

where r is the distance from the centre of the aggregate and d is the space dimension.

Following the other approach, one should plot the dependence of the number of particles contained in a square covering the aggregate on the length of the square side (the so-called sand-box technique). This method employs the dependence of the number, N, of particles in an aggregate on the size, R, of the aggregate (see Ref. 1)

$$N = k_0 \left(\frac{R}{a}\right)^{d_f}, \tag{2}$$

(k_0 is the prefactor and a is the size of the primary particles), because the square side acts as the size of the aggregate. For a fractal aggregate, the experimental points fall on a straight line plotted in the double logarithmic coordinates ($\log N - \log R$) and the slope gives the fractal dimension.

The main advantage of the microscopy techniques is the possibility of determination of many fractal parameters, which provide versatile characterisation of aggregates (*e.g.*, a two-dimensional image of a fractal aggregate can be characterised by seven different fractal dimensions [8]). At the same time, these methods are applicable only to rather loose fractal aggregates with $d_f < 2$ (see above).

Yet another procedure for the determination of d_f of aggregates is based on the estimation of the fractal dimension of their sections. This is a useful method of studying opaque composites. It was substantiated by Miyazima and Stanley [9] who derived an equation for the fractal dimension of the structure (d_{fs}) formed upon intersection of two fractal objects

$$d_{fs} = d_{f1} + d_{f2} - d,$$

where d_{f1} and d_{f2} are the fractal dimensions of the overlapping aggregates.

A section of a fractal object is obtained by intersecting a fractal with a plane. Therefore, the fractal dimensions of a three-dimensional object and its section are related by a simple relationship

$$d_{fs} = d_f - 1.$$

Practical evaluation showed [10] that the fractal dimension of flocs determined using this technique coincided with that found from the three-dimensional structure reconstructed using electron microscopy.

In fact, similar considerations also form the basis for confocal scanning laser microscopy, which recently has been used for the determination of characteristics of fractal aggregates.[11] This method involves the determination of the particle distribution in the focal plane of an optical microscope, which is then used to determine the fractal dimension of aggregates. To obtain more reliable results, the fractal object is scanned in different planes.

However, the most widely used methods are small-angle X-ray [12–15] and neutron [16–18] scattering. The most popular technique is static light scattering,[19–24] which involves the determination of the fractal dimension from the dependence of the scattered intensity on the scattering vector. In the case of dynamic light scattering,[3, 23, 25–27] the fractal dimension is found from the temporal dependence of the average size of the aggregate. Lin and coo-workers [28] first showed that this is a power dependence with the exponent $1/d_f$.

A great body of experimental information on the determination of fractal dimensions has been accumulated to date. Therefore, the fractal dimension measurements themselves are no longer topical. Attention now focusses on the studies of the laws of structural transformations experienced by those systems whose evolution is accompanied by the growth of fractal aggregates in some stage. These investigations are mainly based on the studies of light scattering from aggregates.[29–33]

If a system comprises N particles of the same size, the scattered intensity is given by

$$I(q) = N^2 P(q) S(q), \tag{3}$$

where q is the magnitude of the scattering vector and $P(q)$ is the form factor, which for spherical particles has the form

$$P(q) = \left[24\,\frac{\sin(q/2) - (q/2)\cos(q/2)}{q^3}\right]^2, \tag{4}$$

where $S(q)$ is the structure factor

$$S(q) = \frac{1}{N^2}\sum_{j=1}^{N}\sum_{i=1}^{N} \exp[i\boldsymbol{q}\cdot(\boldsymbol{r}_i - \boldsymbol{r}_j)], \tag{5}$$

where $\boldsymbol{q}$ is the scattering vector and $\boldsymbol{r}_i$ and $\boldsymbol{r}_j$ are the particle coordinates. The structure factor can be expressed through the density correlation function, $C(r)$, of the aggregate

$$S(q) = \frac{1}{N}\left[1 + 4\pi\int_0^\infty C(r) r^2 \frac{\sin(qr)}{qr}\,\mathrm{d}r\right]. \tag{6}$$

The normalising factor $1/N$ is introduced to provide $S(q = 0) = 1$.

From Eqn (6) it follows that the structure factor strongly depends on the density distribution in the system under study. Suppose that the pair correlation function of fractal aggregates in the three-dimensional space is given by

$$C(r) \propto r^{d_f - 3} h\left(\frac{r}{R_g}\right)$$

and that the cutoff function has a Gaussian shape

$$h(x) = \mathrm{e}^{-x^2},$$

where

$$x = \frac{r\sqrt{d_f}}{2R_g},$$

R_g is the radius of gyration of the aggregate. Then, the structure factor can be calculated using an exact analytical expression

$$S(q) = \mathrm{e}^{-(qR_g)^2/d_f} F_1\left[\frac{3 - d_f}{2},\ \frac{3}{2},\ \frac{(qR_g)^2}{d_f}\right], \tag{7}$$

where F_1 is the hypergeometric function.

The shape of the cutoff function has a rather strong effect on the structure factor. Using the exponential cutoff function

$$h(x) = \mathrm{e}^{-\kappa_1 x}, \quad x = \frac{r}{R_g},$$

one gets

$$S(qR_g) = \left(1 + \frac{q^2 R_g^2}{\kappa_1^2}\right)^{(1-d_f)/2} \frac{\sin[(d_f - 1)\mathrm{arctg}(qR_g/\kappa_1)]}{(d_f - 1)(qR_g/\kappa_1)}. \tag{8}$$

The set of cutoff functions also includes the functions employed in the model of overlapping spheres, where

$$h(x) = 1 - \frac{3}{4}\kappa_2 x + \frac{\kappa_2^3}{16}x^3 \quad \text{at} \quad x < \frac{2}{\kappa_2}$$

and

$$h(x) = 0 \quad \text{at} \quad x > \frac{2}{\kappa_2},$$

and the stretched exponent

$$h(x) = \mathrm{e}^{-\kappa_3 x^{\kappa_4}}.$$

Using these cutoff functions makes the expressions for the structure factor of a fractal aggregate more cumbersome.

Experimental studies of the effect of finite aggregate size on the small-angle light scattering intensity were reported.[34, 35] The possibility of reconstructing the cutoff function from the structure factor $S(q)$ was pointed out,[36, 37] which can also be done for polydisperse aggregates provided that the structure factor is measured for a broader interval of q values.

Fractal aggregates of complex structure and the corresponding structure factors were studied by Zhu and White [38] assuming an oscillating radial density distribution in the aggregate. Using such an exotic density distribution, it was found that the model correctly reproduces the experimental scattering pattern obtained for aggregates in a polydimethylsiloxane/paraffin liquid mixture.

Expressions (7) and (8) describe individual aggregates. Colloidal dispersions are always characterised by some aggregate size distribution, or particle number (s) distribution. This complicates the expressions for the structure factor [35] and, hence, comparison of the theoretical and experimental dependences. In particular, calculations [39] of various parameters, which can be determined in the static light scattering experiments, were carried out with the following aggregate size distribution

$$N_s = s^{-\tau} \exp\left[-\left(\frac{s}{\langle s\rangle}\right)^{\beta_s}\right],$$

where τ and β_s are numerical parameters and $\langle s\rangle$ is the average number of particles, and with the stretched exponential cutoff function. The expressions derived are too cumbersome and therefore not presented here.

Usually, static light scattering experiments involve intensity measurements in some range of scattering angles, $a \ll q^{-1} \ll R_g$, corresponding to the so-called small-angle scattering rather than in the whole available interval of scattering angles. In this case, the scattered intensity is given by

$$I(q) \propto (qR_g)^{-d_f}. \tag{9}$$

This relationship permits both the fractal dimension and the radius of gyration of aggregates to be determined.

In dynamic or quasi-elastic light scattering experiments information on the size of an object is obtained by analysing the relaxation times of translational, rotational and 'configuration' diffusion. The theory of dynamic light scattering has been well developed.[40] This method involves measurements of the correlation function of scattered light

$$g^{(2)}(t) = \frac{\langle I(0)I(t)\rangle}{\langle I(0)\rangle^2}, \tag{10}$$

i.e., the time-averaged product of the scattered intensities measured at instants separated by an interval t.

The second-order correlation function (10) is related to the first-order correlation function $g^{(1)}(t)$ as follows

$$g^{(2)}(t) = 1 + G\left|g^{(1)}(t)\right|^2, \tag{11}$$

where G is some function determined by the experimental conditions. The dynamical structure factor for dilute dispersion of particles of the same size is given by

$$S(q,t) = S(q)g^{(1)}(t) = S(q)\left(-Dq^2t\right), \tag{12}$$

where $S(q)$ is the static structure factor and D is the particle diffusion coefficient. In the Stokes approximation the diffusion coefficient has the form

$$D = \frac{kT}{6\pi\eta R_h},$$

where η is the viscosity of the medium and R_h is the hydrodynamic radius of the particle.

Dependence (12) has a clear physical interpretation, namely, the relaxation time $1/(q^2D)$ is the time taken for a spherical particle to travel the distance $1/q$. In the case of non-spherical (*e.g.*, rod-like) objects rotation can affect the scattered intensity at $qR \gg 1$. This also holds for flexible objects (*e.g.*, polymer chains) where conformational relaxation can contribute to the dynamical structure factor at $qR \gg 1$. For most colloidal objects (in the absence of depolarising scattering) only translational motion contributes to the dynamical structure factor at $qR \ll 1$. Usually, the experimental data allow the initial rate of change in the correlation function or the first cumulant to be found

$$\Gamma_1 = -\left.\frac{\mathrm{d}\ln S(q,t)}{\mathrm{d}t}\right|_{t\to 0} = q^2D. \tag{13}$$

Monodispersed systems are rare in occurrence; therefore, the contribution of polydispersity to the system's dynamics should be included. Experiments with polydisperse systems permit the averaged dynamical structure factor to be determined

$$S(q,t) = \sum_{s=1}^{\infty} s^2 N_s S_s(q,t), \tag{14}$$

In this case, the averaged first cumulant is given by

$$\frac{\Gamma_1}{q^2} = \left[\sum_{s=1}^{\infty} D_s s^2 N_s S_s(q)\right] \Big/ \left[\sum_{s=1}^{\infty} s^2 N_s S_s(q)\right] \tag{15}$$

(it will be recalled that the subscript s denotes the corresponding characteristics of the aggregates composed of s particles).

Thus, the measured diffusion coefficient values are averaged over s^2N_s. This complicates processing of experimental data. A more detailed consideration of the problem can be found in, *e.g.*, a review.[26]

Improved dynamic light scattering methods were developed. Recently,[41] it was shown that the so-called time-resolved dynamic light scattering technique allows not only the gel point of the dispersion to be determined but also the critical behaviour of the system during the sol–gel transition to be studied and the mechanism of gel formation and the architecture of gel-forming clusters to be predicted. The scattering spectrum exhibits some characteristic features suitable for identification of the sol–gel transition and obtaining information on the system under study.

In conclusion of this chapter, mention may be made that both static and dynamic light scattering techniques employed in studies of fractal aggregates can be significantly improved. This can be achieved by comparing the results of model light scattering calculations with the experimental data. For this reason, numerical simulation of aggregation of colloidal particles is carried out simultaneously with calculations of light scattering by the growing aggregates. Recently,[42] the temporal evolution of the intensity of small-angle light scattering by the system of aggregating colloidal

particles was numerically simulated. Both irreversible and reversible coagulation of primary particles and aggregates were considered. The probability for the diffusing particles and aggregates to coagulate by collisions was varied over a wide range. It was shown that irreversible aggregation can lead to growth of clusters with the fractal dimension varied from 1.78 (diffusion-limited cluster–cluster aggregation, or DLA) to 2.1 (reaction-limited cluster–cluster aggregation, or RLA). At $qR_g \gg 1$, the scattered intensity depends on the scattering vector as follows

$$I(q) \propto q^{-d_f}.$$

The plot $I(q)$ exhibits a peak which becomes higher as the particle coagulation probability decreases. This points to densification of the particles. In the case of reversible aggregation, the peak appeared in early stages is shifted towards small q values as the time passes. This is accompanied by an increase in the scattered intensity and in the fractal dimension of the aggregates present in the system. Finally, the peak disappears. The theoretical relationships derived in Ref. 42 correctly reproduce the experimental data obtained for aggregates of polystyrene latex particles reported by Giglio *et al.*[43,44] It was pointed out that phenomenological dependences of the type [45]

$$S(q) = S(0)\left(1 + \frac{2}{3d_f} R_g^2 q^2\right)^{-d_f/2}, \qquad (16)$$

which have no extrema, were obtained for the conditions characterised by the significant role of thermally induced restructuring of clusters.

2. Experimental studies of the growth of fractal aggregates

Aggregation processes are studied to solve various problems. We will consider some most important avenues of research into the kinetics of particle aggregation accompanied by growth of fractal objects.

One investigation line is to obtain complete information on the coagulating system and to compare the experimental data with the predictions made using the Smoluchowski kinetic equation. Research in this field has long been carried out. A typical example is provided by the study [46] concerned with the growth dynamics of fractal aggregates composed of 10-nm gold particles. Aggregation occurred upon adding hydrochloric acid to a hydrosol. The rate of particle coagulation was controlled by varying the amount of acid. The temporal dependence of the aggregate size was determined using dynamic light scattering. The fractal dimension of aggregates, d_f, was estimated at 1.9 rather than exactly determined. The aggregate size was found to be time dependent as follows

$$R \propto t^{z/d_f},$$

where $z = 1/(1-\mu)$ and μ is the homogeneity parameter of the coagulation kernel. At high acid concentrations, μ was equal to -0.6. As the concentration of the acid added decreased, the μ value gradually increased to 1. It was pointed out that the limiting value of the parameter μ obtained at high acid concentrations differs from zero ($\mu = 0$ corresponds to the DLA regime). A tendency of μ to unity at low acid concentrations corresponds to the RLA regime characterised by exponential increase in the aggregate size. Hence, the study [46] demonstrated that the experimental kinetics of particle aggregation is in agreement with the predictions of the Smoluchowski theory.

'Workability' of the Smoluchowski equation was confirmed in a number of light scattering studies, in particular, in the experiments on aggregation of 3-nm silica nanoparticles in aqueous solutions at different pH values and temperature (d_f varied from 1.75 to 2.01) [47] and polystyrene latex particles of size 60 and 140 nm dispersed in aqueous solutions in a wide range of changes in the salt concentration in the solution.[48] Both studies revealed good agreement between the theoretical and experimental temporal dependences of the aggregate sizes.

Yet another research avenue is to study colloidal dispersions of more complex composition and the kinetics of aggregation accompanied by growth of fractal aggregates under conditions that differ from both DLA and RLA regimes. This can be illustrated taking the results of studies [49–52] as examples. For instance, easily restructurable aggregates characterised by low fractal dimension were grown in the experimental studies on coagulation of oppositely charged particles of different size and shape.[49,50] Deviations from the DLA and RLA laws were found [51,52] in those experiments where particles coagulated upon adding non-indifferent electrolytes capable of changing the surface charge of the particles. These deviations were ascribed [52] to the short-range repulsive forces that operate in such systems (see Refs 53–55).

The growth dynamics and the fractal dimension of aggregates also depend on the presence of stabilisers (surfactants or polymers) on the particle surfaces. Surfactant modifiers can serve not only as regulators of the rate of coagulation but also initiators of the process. For such systems the laws of aggregation can be significantly different.[56–58] Nevertheless, it should be noted that modification of the particle surface not necessarily affects the fractal dimension of aggregates.[59]

Quite unexpected results were obtained [60] in studies of aggregation of polystyrene latex particles stabilised by poly(*N*-isopropyl)acrylamide. The rate of particle aggregation was controlled by varying the temperature of the system and by adding salt. It was found that the fractal dimension of aggregates increases from 1.8 to 2.7 with increasing the salt concentration and, hence, the rate of coagulation. This change could not be obtained by combining the DLA and RLA regimes. What is more, the experimentally determined laws of changes in the fractal dimension could not be explained by the restructuring of aggregates (DLA-grown aggregates were characterised by a fractal dimension of 1.7 before and of 2.1 after restructuring).

To establish the mechanism of such an unusual aggregation process, the laws of the growth of fractal aggregates of polystyrene latex particles stabilised by sodium dodecylsulfate were studied comprehensively.[61] The experiments involved variation of the particle sizes and the degree of coverage by the surfactant layer. Coagulation of particles was initiated by adding salt. The fractal dimension of aggregates and the temporal dependence of the mass of aggregates were determined using static and dynamic light scattering, respectively. It was established that salt additives affect both the mechanism of aggregation and the structure of aggregates, whereas the adsorption layer of the surfactant affects only the structure of aggregates (more exactly, it mainly affects restructuring of aggregates after completion of aggregation process). Changes in the kinetics of particle aggregation and in the fractal dimension of aggregates were compared with the changes in the potential of interparticle interaction determined in the Derjaguin–Landau–Verwey–Overbeek approximation with inclusion of the adsorption layer of surfactant. It was found that the unusual mechanism of the formation of the fractal structure is governed by a rather complex procedure of particle aggregation. Namely, the primary act of aggregation corresponds to the case where particles come within a distance which is nearly equal to twice the thickness of the adsorption layer. This allows particles to retain lateral mobility, which is responsible for restructuring of aggregates. Only after some time do the particles begin to contact one another, thus losing mobility in the aggregate.

Apparently, the unexpected results obtained in Ref. 60 can be explained by the fact that the authors of this study assumed a linear dependence of the mass of aggregates on time. However, it was found that this not necessarily holds in the case of the complex mechanism of aggregation. In particular, power dependences of the mass of aggregates on time with different exponents were obtained [61] and some deviations from them at certain salt concentration values were pointed out.

Aggregation of 50-nm hematite particles in the presence of adsorbing polymer (polyacrylic acid) was studied.[62] The fractal dimension of aggregates was determined using static light scattering with different cutoff functions. The polymers used had different molecular masses (1.36×10^6 and 3.69×10^4). Three regimes of particle aggregation, *viz*., pre-DLA, DLA and post-DLA were practically implemented. The fractal dimension determined with the exponential cutoff function was 0.1 to 0.2 larger than that found using the Gaussian cutoff function. The fractal dimensions were independent of the molecular mass of the polymer. The fractal dimension of the DLA grown aggregates was 1.84 with the exponential cutoff function or 1.73 with the Gaussian cutoff function. At low polymer content, no DLA regime was attained and the aggregation was reaction limited (growth of more compact aggregates with a fractal dimension of 2.0). Aggregation in the post-DLA regime (excess of polymer) was slow, but the structure of aggregates ($d_f = 1.8$) was similar to the structure formed in the DLA regime.

The studies carried out before Zhang's communication [62] were concerned only with aggregation of polymer-stabilised particles initiated by salt additives [60, 63] or with flocculation using a polymer whose radius of gyration was much smaller than the hydrodynamic radius of the colloidal particles.[64] The fractal dimension greater than 3 [the exponent in the expression for $S(q)$ changed from 2.83 to 3.42] was obtained at a low content of the polymer (fulvinic acids).[63] At a large content of fulvinic acids, the fractal dimension varied from 2.03 to 2.27. Growth of looser structures was explained by the formation of polymer links despite the low molecular mass of the polymer (~ 1000).

Zhang and co-workers [62] also studied [65, 66] aggregation of hematite particles initiated by adding polyacrylic acid using dynamic light scattering. It was found that aggregation occurs due to neutralisation of the charge on the surface of particles by the adsorbing macromolecules. The fractal dimension of aggregates (1.88) was independent of the molecular mass of the polymer.

3. Restructuring aggregates

In most systems the growth of fractal objects is almost without exception accompanied by their restructuring in different stages of aggregation. Usually, experiments are designed to allow for and to carry out a separate study of this process. Theoretical studies on restructuring of aggregates began immediately after performing the first numerical experiments on the growth of fractal aggregates. Initially, densification was treated formally, *i.e*., assuming that particles and aggregates are free to rotate, be bent, twisted, *etc*.; more recent studies were carried out with inclusion of the relative motion of particles in aggregates.[67–69]

Martin *et al*.[26] investigated the kinetics of aggregation of silica particles of radius 11 nm dispersed in aqueous solutions and reported a spontaneous increase in the fractal dimension of aggregates. In these experiments, particle coagulation was initiated by adding a salt. The temporal dependences of the radius and fractal dimension of aggregates were determined using dynamic light scattering. A power-law increase in the mean radius with time at different initial concentrations of particles and different regimes of coagulation was found, which corresponded to conventional kinetics of particle aggregation. The fractal dimension changed from 1.73 for fast (diffusion-limited) to 2.05 for slow (reaction-limited) aggregation. At the same time, it was pointed out that the fractal dimension of the system under study is determined not only by the regime of aggregation but also by some other parameters (*e.g*., concentration and the chemical nature of the salt added). Long-term observations revealed a dramatic change in the fractal dimension of certain aggregates due to restructuring. An analogous restructuring of aggregates also occurred when the dispersion was in a shear flow.

Similar results were obtained in the experiment [70] with silica particles of size 5 and 9.4 nm (aggregation was also initiated by adding a salt). The kinetics of particle aggregation in the DLA and RLA regimes corresponded to that predicted by the Smoluchowski equation with the relevant coagulation kernels. However, the fractal dimension of the DLA-grown aggregates increased to a value of 1.8 after passage of a long time. The change in the fractal dimension was also associated with restructuring of aggregates.

Restructuring of aggregates was also observed in studies of polymer-initiated aggregation [71, 72] (a polymer was added to the solution) and various aerosol systems.[73, 74]

4. Anisotropic aggregates

Most fractal aggregates are anisotropic.[75, 76] This opens up new prospects for studies of their structure and the kinetics of growth.

To characterise anisotropic aggregates, it is possible to introduce two fractal dimensions and the self-affinity exponent. To determine these parameters, one should obtain aggregates with pronounced anisotropy. A good example is provided by aggregates of soot particles and some other highly dispersed aerosols. Here, the prefactor and the fractal dimension can be determined with ease;[77] however, the prefactors obtained much exceeded those found for a conventional RLA model. To eliminate this problem, an extended characterisation of aggregates of soot particles was carried out.[78] The particles were found to be self-affine rather than self-similar objects. Fitting the experimental data for the entire population of aggregates gave conventional values of the fractal dimension ($d_f = 1.7$) and the self-affinity exponent [1] ($A = 0.91$).

In the case of anisotropic particles the static and dynamical structure factors can be expressed as multipole expansions [75]

$$S(q) = \sum_l S_l(q), \tag{17}$$

$$S(q,t) = \sum_l S_l(q) \exp\left[- Dq^2 t - l(l+1)\Theta t \right],$$

where

$$S_l(q) = \sum_{m=-l}^{l} \left| \sum_{i=1}^{N} J_l(\boldsymbol{q} \cdot \boldsymbol{r}_i)\, Y_{lm}(\Omega_i) \right|^2 \tag{18}$$

and $J_l(\boldsymbol{q}\,\boldsymbol{r}_i)$ is the lth order Bessel spherical function, Y_{lm} is the lmth order spherical harmonic, Ω_i is the orientation of the vector $\boldsymbol{r}_i$ determining position of the ith particle with respect to the centre of mass of the aggregate; and Θ is the rotational diffusion coefficient given by

$$\Theta = \frac{kT}{8\pi\eta R_h^3}.$$

The scaling behaviour of terms of the multipole expansion (17) for the aggregates grown in the diffusion-limited and reaction-limited cluster–cluster aggregation regimes and in the diffusion-limited particle–cluster aggregation regime was studied in detail by Meakin *et al*.[75] For cluster–cluster aggregation, they found that the fractal dimension describes the q-dependence of not only the total structure factor but also the terms of the multipole expansion. By contrast, clusters formed by particle–cluster aggregation did not exhibit the same degree of scale invariance.

Relationship (15) for anisotropic aggregates is valid only in the small-q limit ($q \to 0$). However, the scaling behaviour of the second cumulant for anisotropic aggregates changes at $q \to 0$. It is an easy matter to find that the following relation holds for anisotropic aggregates at $q \to 0$

$$\frac{\Gamma_2}{\Gamma_1^2} = Q\left(\frac{\Theta}{D}\right)^2, \tag{19}$$

where Q is a constant; for spherically symmetric aggregates this ratio equals zero.

The optical method [79, 80] of investigation of fractal aggregates is based on their natural anisotropy. The essence of the technique is as follows. The scattered intensity is measured after switching on and off a constant electric field. Switching on the field causes the fractal aggregates to be oriented in space, thus changing the scattered intensity. Switching off the field is followed by disordering of aggregates and the scattered intensity changes again. By analysing the dynamics of changes in the scattered intensity and by comparing the steady-state scattered intensities in the presence and in the absence of external field it is possible to determine the diffusion coefficients of aggregates. Using a number of dispersion samples prepared by successive removal (by, *e.g.*, centrifugation) of aggregates of different sizes, it is possible to determine their fractal dimension. Experiments with silica particles gave a fractal dimension of 2.5.[80] Analysis of experimental data also revealed a linear dependence of the induced dipole moment of aggregates on their size.

Theoretical analysis [81–83] of the laws of relaxation of orientational optical effects showed that the anisotropic structure of aggregates can make itself evident in the orientational turbidimetric effect, which is measured in unpolarized laser beam. The effect manifests itself as a difference between the optical densities of colloidal dispersions in which fractal aggregates are disordered and oriented by the external field. This effect is due to the dependence of the total extinction cross-section of anisotropic aggregates on their orientation. The theory of orientational turbidimetric effect was generalised [84] by inclusion of the interaction between dipoles in the fractal aggregate. The magnitude of the effect was calculated for fractal clusters of different size grown under specific conditions and then evaluated experimentally. Theoretical predictions (in particular, scale invariance of the structure of aggregates and turbidimetric effect) were confirmed by the experiments with 40-nm silica particles. Namely, the dependences of the magnitude of the effect on the aggregate size and on the emission wavelength specifically normalised fell on the same curve.

Yet another method [85] of studying the laws of growth of anisotropic aggregates involves the determination of the kinetics of development and relaxation of birefringence, which is observed in dispersions of fractal aggregates upon application of external electric field. The technique was evaluated taking dispersions of 9.5 nm polystyrene latex particles as examples (particle aggregation was initiated by adding a salt). The fractal dimension of aggregates and the growth rates were in agreement with the corresponding values found for these systems by dynamic light scattering.

5. Aggregation in transient regime

Particle aggregation is carried out in a particular regime. Diffusion-limited cluster–cluster aggregation causes clusters with a fractal dimension of 1.8 to grow; the fractal dimension of the RLA grown clusters can be as large as 2.1. Not only the fractal dimensions but also the functions $f(x)$ determining the cluster size distribution are different. In the case of diffusion-limited cluster–cluster aggregation one has

$$N_s(t)^2 \propto s^{-2} f\left(\frac{s}{\langle s\rangle(t)}\right),$$

and the function $f(x)$ has the form

$$f(x) \approx \mathrm{e}^{-x}.$$

The mean aggregate size varies with time as follows

$$\langle s\rangle(t) \propto t.$$

In the case of reaction-limited cluster–cluster aggregation one has

$$f(x) \approx x^{-1.5}\mathrm{e}^{-x}$$

and $\langle s\rangle$ exponentially increases with time. Usually, the results of theoretical studies of DLA are in good agreement with the experimental data and with the results of numerical simulation. As to RLA studies, agreement is observed only in the initial stages of the process. Deviations from the RLA regime were established in both model [33] and numerical [86, 87] experiments. Namely, the fractal dimension varied with time and the exponential growth of the aggregate size was changed by a power-law process.

Systematic studies of the transition region between diffusion- and reaction-limited cluster–cluster aggregation were carried out.[88–92] Aggregation of polystyrene latex [88–91] and silica [92] particles was initiated by adding a salt. The salt concentration was chosen to deliberately perform experiments in the transient regime of aggregation. Dynamic and static light scattering studies reliably established that the transition does occur. Experimental data were confirmed by the results of calculations using the Smoluchowski coagulation equation with a time-dependent coagulation kernel (kernel parameters were chosen based on information on the interaction between latex particles in electrolyte solutions). The possibility of solving the inverse problem, namely, determination of parameters of the interaction between latex particles from the kinetics of coagulation (more rigorously, from the point of transition from one regime of aggregation to another) was also shown.

Experiments showed [90] that the aggregate size increases linearly with time and that the so-called stability factor, w_c, is related to the fractal dimension

$$d_f = 1.45 + 0.857\ln w_c\,. \qquad (20)$$

This dependence is valid if the stability factor varies within an order of magnitude.

Differences between the $I(q)$ dependences obtained for the DLA and RLA regimes were reported.[91] Experiments on diffusion-limited cluster–cluster coagulation of polystyrene latex particles revealed that the $I(q)$ dependence passes through a maximum at a finite q value. As the process developed, the peak shifted towards small q, which corresponded to spinodal decomposition. Similarly to the results reported earlier for other systems,[43, 93] no peak was observed for the $I(q)$ dependence when the process was performed in the RLA regime. Transient aggregation studies revealed a gradual transition from the RLA to the DLA regime. The change in the regime of aggregation was accompanied by some delay in the appearance of the $I(q)$ peak; development of the coagulation process led to disappearance of the peak.

Studies of various systems using calculations with the Smoluchowski equation for transient regime of aggregation allowed one to choose the coagulation kernels, which best described the experimental kinetics of particle aggregation.[89, 94–97]

6. Anisotropic particles

Most theoretical and experimental studies are carried out using spherical particles. Aggregation of anisotropic particles also causes the formation of fractal structures.[98, 99] This process was studied [100] in detail by experimenting with iron(III) particles 20–30 nm long and 2–3 nm in diameter, which were electrostatically stabilised in the aqueous dispersion. Coagulation of particles was initiated by adding an electrolyte. The characteristics of aggregates were determined using dynamic light scattering, transmission electron microscopy and small-angle X-ray scattering. Experiments revealed the formation of fractal aggregates with $d_f = 1.95$. The temporal dependence of the aggregate size exhibited two linear portions; the growth rate changed after the aggregate size became as large as nearly 300 nm. A tendency to parallel orientation of particles in the aggregate was pointed out. Because of this, aggregates contain rather dense regions, the extent of densification being strongly affected by the rate of coagulation. It is the dense regions that serve as building blocks for the fractal structure of the whole aggregate.

The first theoretical study of diffusion-limited aggregation of anisotropic particles was reported by Meakin *et al.*[101] who

analysed fast and slow rotation of particles in a two-dimensional system with substantially different coagulation probabilities for two different particle orientations. The structure of the growing aggregates was shown to be strongly dependent on the particle rotation rate. Namely, slow rotation of particles with a prescribed orientation causes needle-shaped aggregates to grow, whereas fast rotation or aggregation of disordered particles leads to branched aggregates.

The aggregation of rod-like and fibrous particles and corresponding gel formation was studied.[102] Simple estimates gave expressions for the concentration of the disperse phase at the gel point, the coordinates of the maximum of the structure factor of the dispersion and for the gel density. The relationships obtained differed from the corresponding expressions for spherical particles only in that the cubic root of the particle volume was used instead of the particle radius. Experimental data on the volume fractions of the disperse phase were reported, which corresponded to transition of dispersions of iron(III) hydroxide, clay, rod-like particles imogolite (aluminosilicate fibres), boehmite and silica particles to the gel state. It was found that gel formation occurs at the volume fractions of the disperse phase that are nearly an order (sometimes, two orders) of magnitude smaller than those corresponding to random packing of rods. The fractal dimension of aggregates of rod-like particles depended on their nature and varied from 1.95 for hematite aggregates to 2.35 for boehmite ones.

The depolarised dynamic light scattering technique appeared to be convenient for studies of aggregation of optically anisotropic particles. For systems composed of such particles the depolarised component in the scattered light is independent of the extent of their aggregation. Besides, it was shown [103, 104] that at sufficiently small q values the decay of the correlation function of photons is governed solely by the rotational diffusion coefficient. Experiments on the aggregation of crystals of a (tetrafluoroethylene-*co*-hexafluoropropene) copolymer showed that the correlation function has the form of a stretched exponent

$$g_{\mathrm{d}}(t) = \exp\left[-\left(\frac{t}{\tau_{\mathrm{d}}}\right)^{\beta_{\mathrm{d}}}\right],$$

where τ_{d} is some characteristic time and the parameter β_{d} is related to the fractal dimension as follows

$$\beta_{\mathrm{d}} = \frac{d_{\mathrm{f}}}{3 + d_{\mathrm{f}}}.$$

Crystals of the above-mentioned polymer (size 40 nm) were characterised by a fractal dimension of 2, which was in good agreement with the prediction based on the RLA model.

7. Polydispersed colloids

The effect of particle polydispersity on the structure of fractal aggregates was experimentally studied [105] taking mixtures of virtually monodispersed hematite particles of size 70 and 216 nm as examples. Mixing of two stable dispersions of particles of the same size was followed by their coagulation induced by addition of salt. At the same time, experiments on coagulation of monodispersed particles were carried out. The fractal dimension was determined using three methods based on static light scattering, namely, relationship (9) for the q dependence of the scattered intensity, the Guinier equation for very small scattering angles

$$I(q) = I(0)\left[1 - \frac{1}{3}(qR_{\mathrm{g}})^2\right]. \qquad (21)$$

and correlation of the average mass and the radius of gyration of aggregate at a given scattered intensity $I(0)$. The fractal dimensions obtained were very close (about 1.75) irrespective of whether the system was monodispersed or bidispersed.

Fractal structures are also formed in atmospheric aerosols, which can thus be treated as polydisperse colloidal systems. Atmospheric aerosols and their laboratory-born analogues were studied using various methods.[106] Interpretation of experimental data was complicated by the fact that atmospheric aerosols can undergo essential restructuring owing to absorption of atmospheric water. It was found that the fractal dimension of atmospheric aggregates can vary from 1.5 to 3; the structure factor (prefactor) of fractal aggregates also varied over a wide range. In some cases the fractal dimension increased as the number of particles in aggregates increased. Apparently, this was due to restructuring of aggregates.

8. Search for new systems and methods

Most recently reported experimental studies on fractal aggregates were devoted to searching for new systems suitable for aggregation. For instance, a light scattering study [107] showed that porphyrin molecules form fractal aggregates in aqueous solutions in the DLA regime. The fractal dimension of aggregates of humic acid particles is typical of RLA regime.[108] Aggregation of copper oxide particles initiated by addition of an exotic biopolymer produced by microorganisms was also investigated.[64] The results of studies on the effect of ferrocene additives on the density and fractal dimension of soot aggregates formed during combustion of methane in a laminar diffusion flame were reported.[109] Aggregation of fullerenes C_{60} and C_{70} in a mixed toluene–acetonitrile solution was studied.[110] The aggregate sizes were determined using static and dynamic light scattering. The aggregation process was found to occur reversibly. Sedimentation of aggregates began after they grew to nearly 300 nm. The hydrodynamic radius and the radius of gyration of aggregates were determined. The fractal dimension was 2.1 for C_{70} and 2.9 for C_{60} clusters.

Growth of fractal aggregates from vesicles bound by a special agent (streptavidine) was studied.[111] A feature of the aggregation process was the use of a small amount of binder to provide finite sizes of the growing aggregates; the growth of aggregates ceased after consumption of the whole amount of binder introduced into the system. Static light scattering measurements of aggregates of different sizes gave the same value of the fractal dimension (2.9).

A somewhat different vesicular structure was also observed:[112] vesicles 30–50 nm in diameter were formed from variously functionalised fullerene molecules. Aggregation of such vesicles led to formation of a foam-like structure with cavities of different size. Light scattering and transmission electron microscopy data showed that the growing structure was self-similar with a fractal dimension of 1.4.

A number of studies concerned the laws of the growth of fractal aggregates from particles immediately after formation of the latter in various physicochemical processes. Formation of fractal structures immediately after nucleation of hydrous ferric oxide from 10-nm particles was studied.[113] It was established that the fractal dimension of aggregates of hydrous ferric oxide particles increases from 1.5 to 2 as time passes. A static light scattering study of aggregation of AgI particles formed by mixing of aqueous solutions of $AgNO_3$ and KI was reported.[114] Depending on the salt concentration ratio (the higher the fraction of $AgNO_3$, the greater the d_{f} value), aggregates with fractal dimensions varied from 1.61 to 2.88 grew in solution. A rather smooth dependence of the fractal dimension on the salt concentration ratio was established. Apparently, changes in the component concentrations in the system under study were followed by changes in the particle aggregation regime from DLA to RLA. Restructuring of aggregates cannot also be ruled out. Growth of fractal aggregates from silver nanoparticles formed in γ-irradiated aqueous solutions was studied.[115] Fractal aggregates of size 20 and 100 nm were obtained. Depending on the reaction conditions, the fractal dimension of aggregates changes from 1.7 to 1.8.

Surface-enhanced Raman scattering was proposed as a tool for studying the kinetics of aggregation of colloidal particles.[116] Experiments were carried out with pyridine molecules adsorbed

on the silver bromide surface. Temporal dependences of the Raman scattering intensity were determined for different regimes of particle aggregation. According to the model proposed, the intensity decreases with time obeying a power law

$$I_R \propto t^{(d_f-3)/d_f} \quad (22)$$

The exponent depends on the mechanism of particle aggregation. Fitting the experimental data gave a fractal dimension of 1.81 and 2.16 for colloidal dispersions aggregated in the DLA and RLA regime, respectively.

III. Hydrodynamics of fractal aggregates and their dispersions

1. The hydrodynamic radius of a fractal aggregate

The hydrodynamic properties of fractal aggregates were studied.[117–120] Using numerical simulation and experimental studies, it was established [118,121–123] that the hydrodynamic radius and the radius of gyration of an aggregate are related by a simple relation

$$R_h = \beta_h R_g . \quad (23)$$

For three-dimensional spherical aggregates, the parameter β_h can be expressed through the fractal dimension [121]

$$\beta_h = \left[\frac{2(2+d_f)(d_f-1)^2}{d_f^3}\right]^{1/2} . \quad (24)$$

For aggregates with $d_f = 2.1$, one gets $\beta_h = 1.04$. Other models (see , *e.g.*, Ref. 124) included the dependence of β_h on the number of particles in the aggregate. However, this had little effect on the absolute values of β_h.

Some other values of the parameter β_h were also obtained. For instance, Wiltzius [123] reported β_h values of 1.03 and 0.62 found from calculations based on the Kirkwood–Riseman model (see Ref. 125) for rather large aggregates using a step and an exponential cutoff function, respectively. This indicates a high 'sensitivity' of the hydrodynamic radius to the structure of the aggregate perimeter. The experimental hydrodynamic radius of the RLA-grown fractal aggregates of 3.5-nm silica particles was found to be 0.72, thus lying between the limiting values predicted by theory. These results were considered [122] underestimated because of ignoring possible polydispersity of aggregates in processing experimental data. The β_h value determined with inclusion of polydispersity varies in the range 0.82–0.98 depending on the type of the cutoff function.[122] Numerical simulation [121] (off-lattice RLA model) gave a β_h value of 0.97, which remained virtually constant as the aggregate size changed,[121] whereas calculations [124] in the framework of Brinkman's model assuming a uniform permeability of aggregates gave $\beta_h = 1.23$. Rogak and Flagan [119] solved the hydrodynamic problem using the scattering method with different models of self-similar aggregates and obtained $\beta_h \approx 1$. This approach is applicable only to clusters composed of a small number of particles. The expression relating β_h to the number of particles in the aggregate was extrapolated to the case for large aggregates using a special procedure based on replacement of a group of particles in large aggregates by one spherical particle. Numerical calculations [120] in the framework of Brinkman's model assuming a radially varying aggregate porosity allowed the dependence of the parameter β_h on the fractal dimension and aggregate size to be determined. The β_h values obtained were in agreement with the results of calculations carried out using other models and with the experimental data.

Based on dimension considerations,[126] a simple relation between the radius of gyration and the hydrodynamic radius of aggregate was established

$$\beta_h = k_0^{1/d_f}\sqrt{\frac{2+d_f}{d_f}} .$$

The β_h values calculated using this equation correspond to the results obtained earlier. The dependence of the viscosity of dispersions containing fractal aggregates on the volume fraction of primary particles was also calculated. Viscosity calculations were performed using various models developed to determine the hydrodynamic permeability of porous media.

The hydrodynamic characteristics of a fractal aggregate were calculated numerically [127] and analytically [128] using the Brinkman model for the flow of a fluid inside the aggregate. It was shown [127] that if the fractal dimension of the aggregate is greater than two, structural inhomogeneity has no effect on the hydrodynamic characteristics and the aggregate can be treated as a particle characterised by uniform porosity.

Filippov [129] calculated the hydrodynamic radius of a fractal aggregate using the multipole expansion of the solution of the Stokes hydrodynamic equations. The expansion coefficients were found by numerically solving the corresponding system of algebraic equations. Calculations were carried out with inclusion of viscous fluid slip on the surface of spherical particles constituting the fractal aggregate. The calculated R_h values coincided with the radius of gyration of the aggregate to an accuracy of 5% to 10% for a wide range of change in the number of particles. As should be expected, taking into account the slip effect led to a decrease in R_h. The same approach was also employed for calculating the thermophoresis and electrophoresis velocities of fractal aggregates.[130] They decrease on increasing the number of particles in the aggregate, being for rather large aggregates nearly 10% lower than the corresponding velocities of a single spherical particle.

The problem of heat transfer between a fractal aggregate and its environment is related to the hydrodynamic problem.[131] Calculations were carried out for free-molecular and continuum heat transfer regimes. It was shown that using the radius of gyration as the equivalent radius can introduce large errors, especially for aggregates characterised by small fractal dimension and in the case of free-molecular heat transfer.

The results of calculations of the hydrodynamic drag of fractal aggregates using different equations were compared [132] with the experimental data on the settling velocities of aggregates of different size. The results obtained using the models with radially varying hydrodynamic permeability of aggregates were in agreement with the experimental data.

For aggregates in a gas, the hydrodynamic radius is determined by the Knudsen number

$$\mathrm{Kn} = \frac{l}{d'} ,$$

where l is the mean free path of molecules and d' is the diameter of the primary particles.

Numerical calculations [133] showed that the collision frequency of gas molecules with a small DLA-grown aggregate is virtually independent of the Knudsen number. An increase in the aggregate size causes the effective diameter of collisions to increase in proportion to $N^{0.417}$ and $N^{0.446}$ (N is the number of particles in the aggregate) at Kn = 2 and Kn = 200, respectively.

Collisions of a point particle with fractal aggregates were studied in more detail [134] taking the DLA-, RLA- and ballistic-grown aggregates as examples (restructuring of aggregates was also considered). Scattering of a point particle by the monomer surface was described by the laws of elastic and diffuse scattering and by a cosine curve. Simulation showed that at $d_f < 2$, the collision cross-section, σ, is proportional to the number of particles in the aggregate, N. At $d_f > 2$, the following relation is valid

$$\sigma \propto N^{2/d_f} .$$

The number of collisions of a point particle with the aggregate is independent of the aggregate size at $d_f < 2$ and increases in proportion to N^{1-2/d_f} at $d_f > 2$. The momentum and the angular

momentum transferred from the point particle to the aggregate by collision were also calculated. It was shown that the drag in a rarefied gas is proportional to N at $d_f < 2$ and to N^{2/d_f} at $d_f > 2$. The angular momentum transferred to the uniformly moving aggregate is proportional to N^{1/d_f}.

A general consideration of the problem of the motion of a particle scattered by the fractal structure was reported.[135] According to calculations, the root-mean-square value of the multiple scattering angle increases with an increase in the free path of particles in proportion to l^{d_f}. This indicates that the angular distribution of particles scattered by the fractal medium is narrower than for the non-fractal medium characterised by the same mean free path of the particles. The possibility of determining the fractal dimension of the structure from the shape of the angular distribution of the scattered particles was pointed out.

2. Aggregation in shear flow

Sonntag and Russel [136, 137] pioneered experiments on the growth of fractal aggregates in a shear flow. They experimented with polystyrene latex particles and varied the shear flow rate, particle concentration and the composition of the disperse medium, which determines the parameters of the particle–particle interaction. It was found that the fractal dimension of aggregates weakly depends on the shear rate and the particle concentration. The d_f values obtained (1.8 to 2.5) mainly depended on the particle–particle interaction. The average cluster size (R) was also shown to be related to the shear rate ($\dot{\gamma}$)

$$R \propto \dot{\gamma}^{-\kappa_R}, \tag{25}$$

where $\kappa_R = 0.35$. The aggregate size was independent of the particle concentration.

Relationship (25) can also be derived based on theoretical considerations. Let us represent an aggregate as a set of chains that transfer the mechanical stress from one end of the aggregate to the other end. The chains are characterised by the chemical dimension d_c and by the bending modulus (E) [138–140]

$$E \approx E_1 \left(\frac{a}{r}\right)^{2+d_c}, \tag{26}$$

where E_1 is the elastic modulus of a monomer unit, r is the distance between the chain ends and a is the chain segment length (or the size of primary particles).

Numerical simulation [141, 142] showed that the hydrodynamic stress is localised at the periphery of aggregates. This allows the limiting aggregate size corresponding to the beginning of restructuring induced by hydrodynamic forces to be determined with ease. For a flow with the shear rate $\dot{\gamma}$, the hydrodynamic force is

$$F_h \propto \eta \dot{\gamma} R^2, \tag{27}$$

and the limiting radius is given by

$$\frac{R_r}{a} \propto \left(\frac{\eta a \dot{\gamma}}{E_1}\right)^{-1/(3+d_c)}; \tag{28}$$

then one gets

$$\kappa_R = \frac{1}{3 + d_c}.$$

The parameter E_1 cannot be calculated using the known expressions for the interaction potential of colloidal particles, because this interaction depends on the interparticle distance only. Therefore, the E_1 value is usually chosen empirically as some fraction of the particle–particle interaction.

Expressions (27) and (28) were evaluated [143–145] using numerical experiments with variation of the type of the interaction between particles in the fractal aggregates and the structural organisation of the aggregates ('rigid' and 'soft' aggregates were studied). According to calculations, these relations are valid with a reasonable accuracy for aggregates of different nature. The parameters of the 'soft' and 'rigid' aggregates corresponded to the experimental values found for dispersions of polystyrene latex [136, 146] and silica particles [146] (aggregates of these particles can be treated as the 'soft' and 'rigid' ones, respectively).

A number of theoretical studies [147–156] (most of them involved numerical simulation) concerned the effects of the concentration [147, 148] and Brownian motion [151] of primary particles, walls,[150] hydrodynamic interaction [152] and structure field flow [153–155] on the laws of growth of fractal aggregates in non-uniform fluid flows. Particle–cluster and cluster–cluster aggregation regimes were considered.[147–149, 153–155] The laminar flow and a weak turbulent flow with mixing of the fluid was also simulated.[155] The possibility of obtaining a self-similar size distribution of compact aggregates in shear flow was reported.[156] No self-similar size distribution was obtained for fractal clusters because of exponential growth of the average cluster size. Simulation using a model two-fraction colloidal dispersion with inclusion of shear-induced fragmentation led to steady-state distributions of fractal aggregates in shear flow.[157]

The subject of experimental studies [158–162] was the influence of mixing [158] and shear rate [159–161] on the structure of aggregates growing under the fast and slow coagulation conditions and in the presence of intense Brownian diffusion (see Ref. 162). In the absence of Brownian motion the fractal dimension was independent of the shear rate,[163–165] while in the presence of intense Brownian motion the aggregates exhibited [162] two structural zones with different fractal dimensions, the greater fractal dimension corresponding to the longer length scale. This situation was also numerically simulated,[163] namely, particle aggregation in shear flow was studied assuming either a complete or partial restructuring of aggregates including aggregation in the absence of restructuring. Simultaneously, the intensity of small-angle light scattering by the grown aggregates was calculated in the Rayleigh–Gans–Debye approximation. The results obtained showed that the scattered intensity patterns corresponded to a fractal dimension of 1.8 on short and of 2.1 on long length scale, respectively. Therefore, the fractal dimension of aggregates in shear flow can be changed only on long length scales.

A large number of recent experimental studies were concerned with the laws of growth of fractal aggregates in turbulent flows.[164–166] It was found that the fractal dimension increases with the stirring rate (turbulent flow intensity). This was confirmed by numerical simulation.[166]

3. Sedimentation of fractal aggregates

The sedimentation velocity (v_s) of a dense aggregate composed of s particles is given by

$$v_s = \frac{2\Delta\rho g a^2}{9\eta} \frac{a}{R_h} s, \tag{29}$$

where $\Delta\rho$ is the density difference between the particle and the fluid, g is the free fall acceleration and η is the fluid viscosity. Since the number of particles in a fractal aggregate is related to the aggregate size by relation (2), the sedimentation velocity is

$$v_s = v_{s0} \left(\frac{R}{a}\right)^{d_f - 1}, \tag{30}$$

where v_{s0} is the sedimentation velocity of a single particle.

From relationship (30) it follows that v_s increases as the aggregate size increases. Therefore, for rather small primary particles there is a critical aggregate size such that for any larger size sedimentation dominates Brownian motion in aggregation processes. The critical size, R_s, can be determined with ease assuming that the times taken for the aggregate to travel the average inter-aggregate distance by sedimentation and by Brownian diffusion are equal. Simple estimation showed[167] that

$$R_s \propto a\varphi^{1/4d_f}\left(\frac{3kT}{4\pi\Delta\rho g a^4}\right)^{1/4d_f}, \quad (31)$$

where φ is the volume fraction of primary particles.

In the initial stage of growth, the settling aggregates are small and insensitive to hydrodynamic stress. However, after reaching a certain critical size they can undergo restructuring. There are two ways of determining the critical size. If sedimentation of already grown aggregates occurs, the critical size is found by analogy with the critical aggregate size in shear flow [see expression (28)]: in the case of sedimentation one has

$$F_h \approx 6\pi\eta R v_s$$

and the first critical radius is given by

$$R_r \propto a\left(\frac{3E_1}{4\Delta\rho g a^2}\right)^{1/(1+d_f+d_c)}. \quad (32)$$

The exponent in expression (32) equals ~ 0.25 and the critical radius weakly depends on the elastic modulus of the single unit. When comparing the calculated and experimental data, one should take into account the possibility of restructuring, which causes densification of aggregates and an increase in their fractal dimension. Restructuring of aggregates was both numerically simulated [143, 144] and observed in model colloidal systems;[24, 34, 136, 137, 146, 168] the fractal dimension usually varied from 1.8 to 2.4.

The second critical radius corresponds to the case where sedimentation is accompanied by growth of fractal aggregates. If attractive interparticle forces acting between two collision-coagulated aggregates are smaller than the hydrodynamic force, the resulting structure will be broken and the aggregates will move away from each other. In this case, the limiting aggregate size is determined assuming that the attractive force is equal to the hydrodynamic force. If the molecular attractive force dominates, the bonding force for two spheres (particles) separated by the distance h_s is given by

$$F_b = \frac{Ha}{12h_s^2},$$

where H is the Hamaker constant. In this case, the limiting radius of the settling aggregates is

$$R_b \propto a\left(\frac{1}{16\pi\Delta\rho a^2 h_s^2}\right)^{1/d_f}. \quad (33)$$

It can be determined from experimental data or estimated assuming that the molecular attraction force equals the steric repulsion force. The results obtained from size distribution calculations for the settling aggregates [169, 170] and from model experiments [171, 172] confirmed the existence of the limiting sizes defined by relationships (28) and (33).

A number of experimental procedures for determining the fractal dimension of aggregates using sedimentation analysis is based on the fact that the hydrodynamic radius differs only slightly from the radius of gyration. The deposit density

$$\varphi_s \propto R_h^{d_f-3} \quad (34)$$

was compared [173, 174] with the viscosity of a dispersion of fractal aggregates

$$\eta_d = \frac{n}{(1-b_v\varphi_a)^{c_v}}, \quad (35)$$

where b_v and c_v are some constants in the empirical dependence [175] of the dispersion viscosity on the volume fraction of the solid phase ($c_v \approx 5.2$ and $b_v \approx 0.4$) and $\varphi_a \propto R_h^3$ is the volume fraction of aggregates in the dispersion. The radius of fractal aggregates was estimated from the data on the dispersion viscosity while the fractal dimension was evaluated from the sedimentation volume. The fractal dimension can also be determined using the aggregate viscosity and settling velocity data.[176, 177]

The settling velocity, v_s, of a dispersion is related to the sedimentation volume, V_s as follows [178]

$$v_s = A_0\left(\frac{V_s}{V_0}\right)^{(d_f-1)/(3-d_f)}\left[1-B_0\frac{V_s}{V_0}\right]^{c_v}, \quad (36)$$

where A_0 and B_0 are some constants and V_0 is the sedimentation volume of non-aggregated particles.

Methods of determination of the fractal dimension only from the sedimentation velocity of aggregates of different size, characterised by the same d_f value were proposed.[179, 180] They involve a special procedure for processing experimental data [180] followed by finding a correlation between the sedimentation velocities of two fractal aggregates and a third aggregate formed from the first two aggregates.[179] (It should be noted that modern methods allow the particle aggregation process to be monitored with ease and are therefore often used for practical purposes,[181] in particular, for preparation of aerosols possessing high sedimentation stability.) Given a constant number of particles, from relationship (30) it follows that the sedimentation velocities of the three fractal aggregates must be related as follows

$$v_{s1}^{d_f/(d_f-1)} + v_{s2}^{d_f/(d_f-1)} = v_{s3}^{d_f/(d_f-1)}, \quad (37)$$

By measuring the settling velocities of the aggregates it is possible to unambiguously determine their fractal dimension. Experiments carried out following the design mentioned above gave $d_f = 1.97$ and 1.19 for aerosol particles of soot and magnesia, respectively. These values are in good agreement with those found for the same systems using electron microscopy.

It is possible to determine the fractal dimension by studying the sediment morphology.[182] However, this approach can be practically implemented only when using non-destructive methods of investigation.

If aggregates are composed of small particles or if the density difference between the disperse phase and the disperse medium is small, sedimentation can slow down due to thermal motion of particles and aggregates. Since in the gravitational field the local concentration of monomers varies with height, the characteristic aggregate size will also change with height.[183] By measuring the density of the disperse phase and the aggregate sizes at different heights one can determine the fractal dimension and draw some conclusions about salient features of structural organisation of aggregates.

Sedimentation of colloidal dispersions is not completed by the formation of loose deposit. Usually, the height of the deposit layer slowly decreases with time due to densification of fractal aggregates. The consolidation dynamics were studied by Potanin and Russel [184] who preliminarily established that the bulk viscosity, η_v and the yield stress, P_c, of the deposit (fractal aggregates) are given by

$$\eta_v \propto \left(\frac{1-\varphi}{\varphi_m}\right)^{-\kappa}\varphi^{\gamma_\eta}, \quad (38)$$

$$P_c \propto \left(\frac{1-\varphi}{\varphi_m}\right)^{-\kappa}\varphi^{\gamma_P},$$

where $\varphi_m \approx 0.61$ is the limiting volume fraction of filling and κ_φ is a fitting parameter,

$$\gamma_\eta = \frac{3+2d_c}{1-d_f},$$

$$\gamma_P = \frac{3}{3 - d_f}.$$

The results of calculations using relations (38) are in good agreement with the experimental data [185] for oleic acid stabilised by alumina particles. The best agreement with the experiment was achieved using a two-fraction model for the sedimenting dispersion, which deals with the deposit itself and the dispersion, which settles without formation of an elastic network.

4. Fractal gel rheology

Recently,[186] a typical example of a detailed rheological study of a gelating colloidal dispersion was reported. The subject of this investigation was a colloidal dispersion of 43-nm silica particles. Flocculation was initiated by adding a salt. The dispersion structure was determined using small-angle X-ray scattering while the storage and loss moduli were determined by oscillation shear rheometry. The scale range of surface fractality was found; however, the fractal dimension was not determined. It was shown that an elastic gel network is formed as time passes. It was established that a slow process proceeds in the system, which results in the change (namely, an increase) in the gel storage modulus but leaves the local structure of the gel virtually unchanged. Shear-induced breakdown of the gel network causes no significant changes in the local structure of the dispersion, whereas the storage and loss moduli decrease substantially. The kinetics of recovery of the moduli mentioned above, measured after shear relieving, differs from the kinetics of growth of the same moduli in the course of flocculation. The laws established are characteristic of fractal colloidal gels of different nature. In particular, the experimentally observed [187] rheological behaviour of a gel of protein molecules was explained only using the fractal approach.

Based on a model treating a gel as an ensemble of contacting fractal aggregates, a simple relation between the elastic modulus of gel and the volume fraction of particles was obtained [14]

$$E_e \propto \varphi^{(1+\zeta)/(3-d_f)}, \tag{39}$$

where ζ is the parameter responsible for the size dependence of the elastic constant of a fractal object (K_e) [188]

$$K_e \propto \frac{K_0}{R^\zeta}. \tag{40}$$

Since then, the elastic and rheological characteristics of gels have been analysed with inclusion of the concept [139, 140] of elastic chains, which are responsible for elastic energy transfer in aggregates and characterised by the chemical dimension.

Considerable attention in theoretical studies has been paid to the so-called weak gels composed of nanoparticles. The formation of loose fractal aggregates in these systems causes gelation even at very low particle concentration (2 vol.% – 3 vol.%). Such systems possess unusual rheological properties. For instance, two regimes of Newtonian flow of dispersions of silica particles at low and high shear stress can differ in viscosity by nine orders of magnitude. At the same time, it is possible to analyse these systems theoretically. The rheological properties of such gels have been the subject of a large number of studies (see , *e.g.*, Refs 138 and 189 – 195).

At low shear rates, the viscosity of a gel is determined by relaxation processes related to breakdown and nearly complete reformation of interparticle bonds. As the shear rate increases, stress overshoot occurs. In this case the energy dissipation mechanism changes. The system goes to the state of a dispersion of hydrodynamically interacting fractal aggregates. In fact, the system seemingly goes from the 'solid-like' to the 'liquid-like' state.

Since in this case the interparticle interaction plays the determining role, the rheological characteristics depend not only on the gel structure but also on the parameters of the interparticle interaction. The most important parameters are the bonding energy, U_c; the bonding force, F_c; and the force constant

$$k_{el} = \frac{d^2U}{dh_s^2} = k_g \frac{F_c}{h_c} \approx k_g \frac{U_c}{h_c^2}, \tag{41}$$

where U is the potential of the interparticle interaction, h_s is the distance between the particle surfaces and h_c is the distance between the particle surfaces at the potential well minimum.

From the equations for the balance of forces and the energy balance one can derive [195] the dependences of the rheological characteristics of weak gels on the volume fraction of particles of the disperse phase.

In the case of oscillating small-amplitude perturbations, the storage modulus is given by

$$G' \propto c_g k_g^{1/2} c_1^{-1} \frac{F_c}{a^2} \varphi^{\gamma_G}, \tag{42}$$

where c_g is a constant of the order of unity,

$$c_1 = \frac{U_c}{kT} \exp\left(-\frac{z_c U_c}{kT}\right)$$

(z_c is the coordination number of the particles in the aggregate) and

$$\gamma_G = \frac{7 + 2d_c - 2d_f}{3 - d_f}.$$

At low shear rates, the dispersion viscosity is

$$\eta \propto c_\eta c_1^{-2} \tau_0 \frac{F_c h_c}{a^3} \varphi^{\gamma_\eta}, \tag{43}$$

where c_η is a constant,

$$\tau_0 = \frac{kT}{6\pi\eta_0 a^3}$$

is the characteristic time of particle diffusion in the disperse medium and η_0 is the viscosity of the disperse medium and

$$\gamma_\eta = \frac{7 + 3d_c - 2d_f}{3 - d_f}.$$

At high shear rates, the effective viscosity is given by

$$\eta = \eta_0 \left(1 - \frac{\varphi_a}{\varphi_m}\right)^{-2.5\varphi_m} + \frac{1}{\dot\gamma} c_\eta \frac{F_c h_c}{a^3} \varphi_a^2 \left(\frac{\varphi}{\varphi_a}\right)^{(5-2d_f-d_c)/(3-d_f)}, \tag{44}$$

where $\varphi_a = \varphi/\varphi_i$ is the volume fraction of aggregates and $\varphi_i \approx (R_g/a)^{d_f-3}$ is the volume fraction of particles in the aggregate. The former parameter depends on the shear rate and aggregate strength and can be determined using the relationship

$$\frac{5\pi}{2} \eta \dot\gamma R_g^2 \approx F_c \left(\frac{\varphi}{\varphi_a}\right)^{1/(3-d_f)}, \tag{45}$$

corresponding to the case where the hydrodynamic stress applied to the aggregate equals the ultimate strength of the aggregate. The model correctly reproduces the experimental data. In particular, analysis of Eqn (44) revealed a Newtonian rheology of gel at high shear rates.

The hypothetised gel flow mechanism [195] was confirmed [196] by numerical simulation under constant shear. Gel was shown to have a yield point and three flow regimes corresponding to increasing stress were revealed. At low strain, no stress overshoot occurs and the system is in viscoelastic flow state. An increase in the strain applied causes fragmentation of the system into large

aggregates and transition to the viscoplastic flow state. This favours further fragmentation of aggregates and then the system goes to the pure viscous flow state.[197]

The dependences obtained [198] for a two-dimensional system of colloidal particles in a complex potential with inclusion of bending elasticity of the interparticle bonds are similar to relations (42) – (44). The dynamics of gel in shear flow were simulated by the Monte Carlo method. The formation of a fractal gel in the system was followed by applying a shear strain. The temporal evolution of the stress developed in gel and the dependences of the stress on the relative deformation and on the steady-state shear rate were traced. Most dependences showed a power-law behaviour, which is typical of fractal structures. Analogous power-law dependences were obtained from similarity considerations, which also allowed the relations between the exponents and the fractal parameters of gel to be followed. Fragmentation studies of fractal aggregates in shear flow showed that this process is to a great extent determined by the bending elasticity of the interparticle bonds.

IV. Optical properties of fractal aggregates

In Section II, structure-dependent peculiar features of small-angle light scattering were considered assuming single scattering and small sizes of primary particles constituting fractal aggregates compared to the emission wavelength.

A study going beyond the scope of this approximation was reported.[199] To include the multiple scattering effects and the fact that the particle size is comparable with the emission wavelength, the light scattering intensity was calculated in the framework of the Mie theory. Each scattering particle in the aggregate was considered as being in some effective medium characterised by a refractive index corresponding to the average aggregate density. The approach was developed [200] with allowance for the fact that the optical characteristics of the effective medium containing the scattering particles vary with the fractal aggregate density. As a result, the form-factor responsible for the scattering by a single particle appeared to be position-dependent, thus affecting the total scattered intensity. The method proposed allows additional information to be extracted (in particular, not only the fractal dimension but also the aggregates sizes were determined).

This approach was experimentally evaluated [201] taking light scattering by aggregates of 0.8-μm latex particles as an example. Experiments involved variation of the concentration and the extent of aggregation of primary particles. Using the Mie theory for the description of scattering by single particles, a greater body of information was obtained from both small-angle and large-angle light scattering data. This allowed not only the fractal dimension of aggregates but also the aggregate size distribution to be determined.

Interesting results were obtained in studies on the behaviour of electromagnetic radiation in fractal aggregates and on the spectrum of the scattered radiation, especially in the presence of nonlinear effects.

The optical properties of fractal aggregates were first studied by Shalaev and Stockman [202] who calculated some optical characteristics in the self-consistent approximation with inclusion of the dipole – dipole interaction between monomers. It was shown that fractal aggregates possess unique optical properties, which differ from the properties of single particles and continuous media. The formation of a fractal causes broadening and splitting of the characteristic lines of the primary particles in the absorption spectrum; however, these lines remain centred near their initial positions, which correspond to the minimum absorption of the fractal. Therefore, the lines can still be treated as resonance ones, which is associated with a fast decrease in the fractal density on going towards its periphery [see Eqn (1)].

Broadening of the lines of the metallic particles forming fractal aggregates was confirmed experimentally (see , *e.g.*, Ref. 203). It is used for monitoring the growth of aggregates in colloidal dispersions even under very fast aggregation conditions.[204, 205] The theoretical approach [202] was developed by Karpov *et al.*,[206] who provided an explanation for all features in the spectra of aggregated colloidal silver particles. In particular, it was found that the second peak in the absorption spectrum of a colloidal dispersion is due to two predominant geometric parameters of aggregates (the size of primary particles and the distance between neighbouring particles) rather than specific resonances in the ensemble of particles. These parameters predetermine the increase in the spectral density of the surface plasmon resonances in a specific wavelength range, which manifests itself in the spectra of sols characterised by rather narrow size distribution of the primary particles (5 to 25 nm).

Yet another important property of fractals is production of surface-enhanced Raman scattering (SERS) by impurity sites.[203] This provides an explanation [207] for the experimental observation of the strongest SERS signal from aggregated metallic particles in colloidal solutions.

Studies on the nonlinear optical properties of fractal aggregates of metallic particles showed that aggregation causes a dramatic enhancement of the nonlinear optical response in the region of plasmon resonance characteristic of single metallic particles.[202, 208 – 221] When the frequency of incident radiation is off resonance, the decay rate of the absorption of a fractal aggregate is lower compared to single particles while the absorption coefficient per particle increases. The imaginary part of the polarisability of a particle in the cluster is related to the detuning, Δ, by the following power-law dependence [210]

$$\chi''(\Delta) \propto a_p^2 (a_p \Delta)^{d_o - 1}, \tag{46}$$

where a_p is the distance between primary particles and d_o is the optical spectral dimension (this parameter lies between 0.3 and 0.6 for different types of fractals). From this relationship it follows that the frequency dependence of the particle's response in the aggregate dramatically differs from the resonance dependence for a single particle. Namely, absorption of the incident wave far from resonance is still high and slowly decreases obeying a power-law dependence as the frequency detuning increases. In some cases, the absorption cross-section increases so greatly that it is more appropriate to describe the situation in terms of the transparency – opacity transition in fractal aggregates.[222]

The results of calculations of the absorption coefficients of fractal and non-fractal aggregates of metallic particles were presented in a comprehensive study [223] of clusters grown in different aggregation regimes. According to calculations, the absorption spectrum of fractal aggregates must have a complex pattern in contrast to the absorption spectrum of non-fractal aggregates, which exhibits a single sharp maximum. For fractal aggregates, the absorption maximum no longer corresponds to the resonance frequency and there is a system of absorption maxima whose positions and intensities are governed by the aggregate structure and by the number of particles in the aggregate.

Fractal aggregates can also sustain optical (dipolar) eigenmodes,[210] which can be localised in some range of wavelengths that are shorter than the emission wavelength.[210, 214] This favours concentration of the electromagnetic energy in the domains whose size is smaller than the diffraction limit of conventional optical devices.

The dispersion equation for the eigenmodes of a fractal aggregate has the form

$$\lambda \propto a_p (a_p^3 \Delta)^{(d_o - 1)/(3 - d_f)}, \tag{47}$$

where λ is the emission wavelength.

Near the resonance frequency ($a_p^3 \Delta \ll 1$,), the dipolar eigenmode is delocalised. As the frequency detuning increases ($a_p^3 \Delta \approx 1$), the eigenmode becomes well-localised at the wings of the absorption bands, *i.e.*, $\lambda \approx a_p$. Localisation of optical excitations favours creation of strong local fields, which leads to giant

enhancement of resonant Rayleigh and Raman scattering and nonlinear light scattering [215–217, 224, 225] observed in colloidal dispersions of some metals. Photomodification of fractal aggregates of silver particles [226] was also explained by localisation of optical excitations.

The results of calculations of dipolar modes localised on fractals are presented in Fig. 1. The local field intensity distributions (shown in Fig. 1 are the isolines corresponding to different electromagnetic field intensities) clearly indicate localisation of the electromagnetic field on the fractal object.

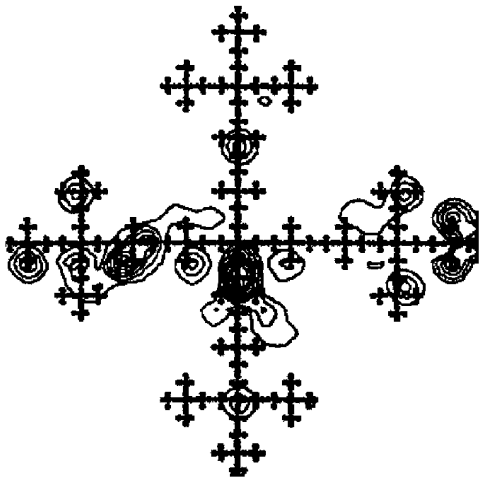


Figure 1. Electromagnetic field intensity distribution on a model fractal aggregate.[223]

The typical size of fractal aggregates composed of nearly 10-nm particles does not exceed the emission wavelength in the optical or IR spectral region. Therefore, such aggregates can be treated as elementary dipoles. Nevertheless, their nonlinear optical characteristics are to a great extent determined by fluctuations of the electromagnetic field inside the aggregates. The corresponding numerical calculations [214, 227–233] showed that the zones of large fluctuations are localised in different small domains of fractals and their positions vary as the emission wavelength varies.

Estimation of the enhancement factor gave

$$G_e \approx \delta_r \left(1 + \frac{\Delta^2}{\delta_r^2}\right) |\chi''(\Delta)|, \qquad (48)$$

where δ_r is the reciprocal Q-factor of resonance, which is determined by resonance amplitude and width. As can be seen, the enhancement factor can be very large at $\Delta \gg \delta_r$.

The calculated dependences of the enhancement factor for different ensembles of particles (regular packs and fractal aggregates of metallic silver particles characterised by a fractal dimension of 1.78) are presented in Fig. 2. As can be seen, the enhancement factor increases to the greatest extent in the case of fractal aggregates. Local enhancement of electromagnetic waves can be explained as follows. In spite of a loose structure, fractal aggregates are characterised by a high probability of finding several particles near a given particle. This is due to the fact that the correlation function of a fractal structure decreases regardless of how the origin of coordinates is chosen.[1] Because of this, neighbouring particles in fractal structures are always strongly coupled. As a result, at any orientation and polarisation of the field there are resonant ensembles of particles, which causes excitation of localised optical modes far from resonance.

Thus, a broad spectrum of localised resonance modes of a fractal aggregate is due to the dipole–dipole interaction between constituent particles. Localisation of modes in different randomly

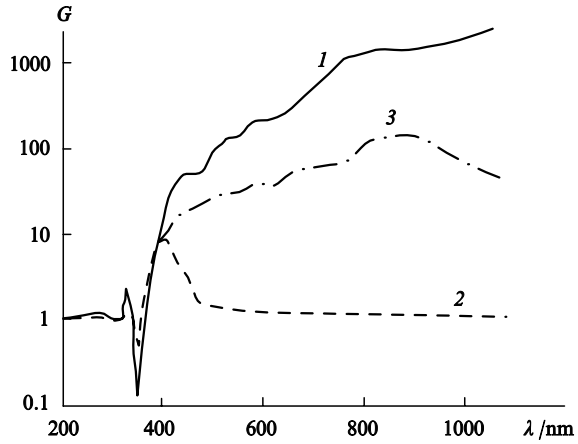


Figure 2. Enhancement factor as a function of the wavelength for fractal aggregates (*1*), randomly distributed metal particles with the same packing density (*2*) and close-packed metal particles (*3*).[223]
The total number of particles in systems is 500. Calculated using the parameters for silver.

located cluster domains causes large local fluctuations of the field and the appearance of 'strong-field' and 'weak-field' domains. In the case of fractal colloidal aggregates of nearly 10-nm silver particles the localisation length varies with the emission wavelength and equals ≈ 100 nm in the blue spectral region and 20 nm in the near IR region.

Shalaev [223] reported the results of calculations of the enhancement factors of other nonlinear optical effects in fractal aggregates (four-photon scattering, second optical harmonic generation and Raman scattering). The enhancement mechanism of nonlinear optical effects is analogous to the mechanisms of localisation of optical radiation and enhancement of local fields (see above).

Predictions of giant enhancement of the nonlinear optical properties of single particles [202, 206–221] aggregated into fractal structures were experimentally tested in the studies of four-photon scattering and nonlinear refraction and absorption.[234, 235] Aggregation of initially isolated particles into fractal aggregates led to an increase in the conversion factor of four-photon scattering by a factor of 10^6 and to enhancement of nonlinear refraction and absorption by a factor of 10^3. Localisation and large fluctuations of local fields in fractals were observed using near-field scanning optical microscopy.[214, 231–233] Experiments [231] were carried out with fractal aggregates ($d_f = 1.78$) of 10-nm silver particles. The aggregates were excited by laser radiation at 488 and 514.5 nm. It was established that the field localisation length is 60 to 140 nm, which is in good agreement with the results of calculations.

The list of the nonlinear optical properties of fractal aggregates considered above is far short from being complete. Experimental evidence of nonlinear gyrotropy of fractal silver clusters due to non-local interaction and its enhancement upon aggregation of silver nanoparticles in a colloidal solution was also reported.[236] Using a specially developed procedure, the contributions of the local and non-local effects to gyrotropy were distinguished. Measurements showed that aggregation of particles into fractal aggregates with $d_f = 1.7$ causes a substantial increase (by about two orders of magnitude) in the contribution of nonlinear gyrotropy.

Localisation of dynamic excitations on disordered structures (in particular, fractals) is a universal property and plays a significant role in many physical processes.[237–241] In addition to localisation of light-induced dipolar excitations, the fractal structure also favours 'trapping' of electromagnetic radiation (light).[217] The light 'trapping' mechanism is similar to the mechanism of localisation of electromagnetic field (see above). At the same time, a somewhat different mechanism of light trapping in a fractal aggregate was reported.[242] This mechanism 'works' in the case of

rather large aggregates and is associated with the predicted [243] strong localisation of light in close-packed granulated media due to the motion of photons along loop trajectories. This light localisation mechanism requires that the aggregate be composed of weakly absorbing particles, the photon wavelength be comparable with the aggregate size and the positions of particles in the cluster be strongly correlated. In this case, at low fractal dimensions of aggregates (a critical d_f value of 2 was obtained [242]) this trapping mechanism also leads to high concentration of the electromagnetic field in fractal aggregates, thus providing an explanation for high reactivity of nanoparticles in fractal aggregates.[242]

The fractal structure of aggregates is also responsible for enhancement of the Rayleigh resonant scattering of electromagnetic radiation. The corresponding numerical and analytical calculations were reported by Shalaev, Botet and Jullien.[215] The enhancement factor of the Rayleigh scattering

$$F_R = \frac{\sigma_s}{N\sigma_{s1}}$$

(σ_s is the scattering cross-section for a fractal aggregate composed of N particles and σ_{s1} is the scattering cross-section for a single particle) depends on the fractal dimension and the aggregate size.

For small aggregates one has

$$F_R \propto \frac{N}{a_p^3\delta_r}(a_p^3\Delta)^{d_o+1}. \quad (49)$$

For large aggregates
at $d_f < 2$ one has

$$F_R \propto \frac{(a_p/\lambda)^{-d_f}}{a_p^3\delta_r}(a_p^3\Delta)^{d_o+1},$$

at $d_f = 2$ one has

$$F_R \propto \frac{(a_p/\lambda)^{-2}}{a_p^3\delta_r}\ln[(ka_p)^2N](a_p^3\Delta)^{d_o+1},$$

and at $d_f > 2$ one has

$$F_R \propto \frac{(a_p/\lambda)^{-2}}{a_p^3\delta_r}N^{1-2/d_f}(a_p^3\Delta)^{d_o+1}, \quad (50)$$

In conclusion, it should be recalled that aggregates of conducting particles in composition materials near the percolation threshold also have a fractal structure. Therefore, percolation systems are also characterised by fluctuations of electromagnetic field and possess nonlinear optical properties.[223] The nature of the magnetic field fluctuations in and nonlinear optical properties of percolation systems has much in common with the corresponding features of fractal aggregates. Because of this, we leave the percolation systems out of our consideration.‡

V. Capillary phenomena in fractal systems

1. Wetting of fractal surfaces

The contact angle on a fractal surface greatly differs from the contact angle on a smooth surface. Theoretically, the contact angle on the fractal surface was determined by Hazlett [245] who studied the case where the droplet size exceeded the length scales on which the scaling relations are valid. This situation is typical of macroscopic systems. The expressions derived for the contact angle on the fractal surface were confirmed experimentally.[246–249] Here, we will present the relationship for the contact angle, which corresponds to a more general case [250] where the droplet size is comparable with the scale range of surface fractality of the substrate. In this case, the contact angle depends on the effective radius, R_d, of the droplet and is given by §

$$\cos\theta_f = \cos\theta_0\left\{\left[\frac{1-(\gamma_{02}/\gamma_{01})(d_2/d_1)^{2-d_f}}{1-(\gamma_{02}/\gamma_{01})}\right]\left(\frac{d_1}{R_d}\right)^{2-d_f}\right\}, \quad (51)$$

where d_1 is the size of the molecules of the liquid; d_2 is the size of the molecules of the gas (or equivalent phase); $\cos\theta_0 = (\gamma_{02}-\gamma_{01})/\gamma_{12}$, θ_0 is the contact angle on the smooth surface and γ_{01}, γ_{02} and γ_{12} are the energies of the liquid/solid, gas/solid and gas/liquid interfaces, respectively. If the droplet size exceeds the longest length scale from the scale range of surface fractality, R_d should be read as denoting the latter parameter.

From relationship (51) it follows that an increase in the droplet size causes the cosine of the contact angle to increase in absolute value. This means that the droplets increasingly better (or worse) wet the surface as the droplet size increases. Deterioration of wetting of fractal surfaces was confirmed experimentally.[246, 247]

Fractal surfaces possessing very high water- and oil-repellent abilities were reported.[248] The results obtained in a large series of experiments on the water- and oil-repellent properties of fractal surfaces were discussed.[249] To impart these properties to the surface of anodised aluminium with $d_f = 2.19$, it was treated with perfluoroalkyltrichlorosilanes and perfluorinated monoalkyl phosphates, respectively. The dependences of the contact angle of a water/ethanol mixture on the smooth and fractal surfaces of anodised aluminium treated with various modifiers are shown in Fig. 3. As can be seen, the contact angle on the smooth surface gradually increases as the surface tension increases, while in the case of the fractal surface the regions of slow change in the contact angle are separated by a discontinuity region. Figure 4 presents a correlation between the contact angle on the fractal surface and the contact angle on the smooth surface. The experimental data are well fitted by the equation

$$\cos\theta_f = \cos\theta_0\left(\frac{d_1}{R_d}\right)^{2-d_f}, \quad (52)$$

which is a particular case of relationship (51).

The fractal nature of the substrate affects not only the contact angle. Investigations of capillary phenomena on fractal surfaces require some relationships to be revised. In particular, the

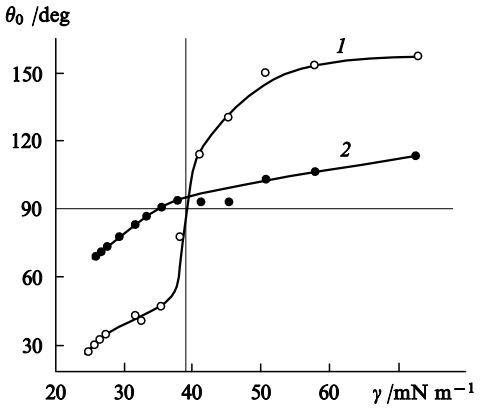


Figure 3. Contact angle of a water/ethanol mixture on a smooth (*1*) and fractal (*2*) anodised aluminium surface treated with various modifiers as a function of the surface tension of the mixture.[249]

‡ Readers who are interested in this problem are addressed to a review,[244] which presents a comprehensive treatment of these effects.

§ The fractal dimensions of surfaces will be also be denoted as d_f. We believe this should not cause any misunderstanding.

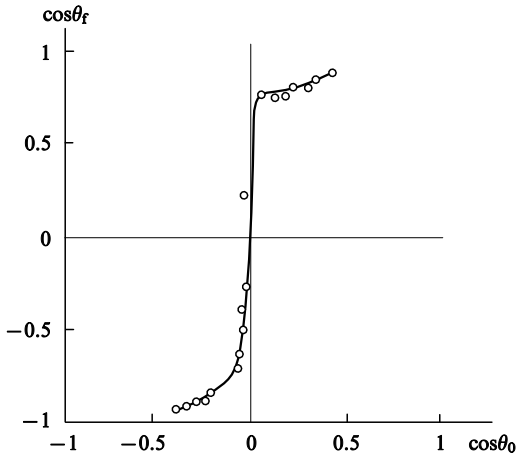


Figure 4. Correlation between the contact angle on the fractal surface and the contact angle on the smooth surface for water/ethanol mixture.[249]

possibility of significant changes in the kinetics of heterogeneous nucleation on fractal surfaces was pointed out.[250] In addition to the classical chemical mechanism of manifestation of the Rebinder effect, yet another mechanism becomes possible [251, 252] in the case of wetting of a metal surface with an eutectic mixture of metals or with some other liquid metal. It is believed [251, 252] that high roughness and the fractal structure of the interface can favour creation of a high concentration of photons in the region of metal/metal or metal/eutectic mixture contact. The high photon concentration may cause a mechanical disruption of the surface of solids.

Wetting studies of fractal surfaces are closely related to the problem of determination of the characteristics of porous bodies. To solve this problem, two approaches were developed. One of them is based on capillary condensation on fractal surfaces (wetting of a porous body), while the other is based on a mercury porosimetry technique (intrusion of a nonwetting fluid into a porous medium).

At first, consider the problem of intrusion of a nonwetting fluid into a porous body, because it is somewhat simpler.¶ As mercury intrudes a nonwetting porous body, the first to be filled are those pores whose radius of curvature, r_h, meets the condition

$$r_h \geqslant \frac{2\gamma_h|\cos\theta_0|}{p}, \tag{53}$$

where p is the pressure of mercury, γ_h is the surface tension of mercury and θ_0 is the contact angle on the smooth surface. This relationship has a simple physical meaning, *viz*., for a pore to be filled with mercury, the external pressure must exceed the capillary pressure. Here, the radius of curvature determined by the sign of equality in relation (53) acts as the length scale in measuring the fractal surface area. The surface area, Σ, of the mercury/porous body interface is determined from the work W_h done in intruding mercury, which is fully spent for an increase in the interface area,

$$W_h = -\Sigma\gamma_h\cos\theta_0 = -\int_0^V p\,\mathrm{d}V, \tag{54}$$

where V is the volume of mercury intruded in the porous body.

The fractal dimension of the surface of the porous body is determined from experimental data using the equation

$$d_f = 2 - \frac{\mathrm{d}\ln\Sigma(r_h)}{\mathrm{d}\ln r_h}. \tag{55}$$

This approach was proposed by Neimark.[255] A somewhat different method of determination of the fractal dimension of a model porous body was developed earlier,[256] but it is applicable to particular cases only. The necessity of refinement of relation (55) was pointed out,[257] because a part of the mercury surface does not contact the solid phase. More accurate relationships allowed one to attain agreement between the data on the fractal dimensions of porous bodies obtained using mercury porosimetry and adsorption techniques.

It should be noted that such a refinement is not always necessary. The need for refinement is most probably due to poorly pronounced fractal structures of the porous bodies under study. One should employ a specific procedure (see Ref. 258) for choosing those portions in the $\Sigma(p)$ plot that correspond to the fractal structure. Correct choice of such portions allows the fractal dimensions of various objects (soot, aerogels) determined from mercury porosimetry data [258] to be in agreement with the values found using small-angle X-ray scattering and adsorption methods.

A capillary condensation based version of the adsorption technique was also proposed.[255] The method assumes that a sufficiently thick adsorption film covers the whole surface of a porous body. The surface area of the film/vapour interface is governed by the vapour pressure; the radius of curvature of the meniscus acts as a 'probe' size and is given by

$$r_l = \frac{2\gamma_l V_m}{kT\ln(p_s/p_v)}, \tag{56}$$

where γ_l is the surface tension of the liquid, V_m is the volume of the molecule, p_s is the saturated vapour pressure and p_v is the current vapour pressure. The expression for the pressure dependence of the surface area, Σ_l, of the liquid/vapour interface can be found from the work done in forming the interface and has the form

$$\Sigma_l = \frac{RT}{\gamma_l}\int_{\Gamma}^{\Gamma_{max}} \ln\left(\frac{p_s}{p}\right)\mathrm{d}\Gamma, \tag{57}$$

where Γ is the adsorption (in moles) and Γ_{max} is the maximum adsorption. The fractal dimension is then determined from Eqn (55) using the radius r_l instead of r.

A modified capillary condensation method was reported.[259, 260] However, it cannot be considered rigorously substantiated.

2. Restructuring of aggregates

Capillary phenomena play a significant role in the evolution of fractal aggregates. There are two types of capillary phenomena. The first type includes condensation of liquids on aerosol fractal aggregates. Capillary forces acting at the liquid/vapour interface can cause changes in the aggregate structure provided low strength of fractal aggregates. The second type of capillary phenomena is responsible for the evolution of aggregates due to 'sintering' of particles.

Experiments [261, 262] revealed changes in the structure of aggregates [261, 262] exposed to cyclic variation of the relative humidity of the atmosphere. At first, experiments were carried out to obtain qualitative information. Detailed studies [263] involved (i) variation of the composition of aerosol soot particles and of the duration of condensation–evaporation cycles and (ii) measurements of the fractal dimension of aggregates at different instants. Based on the results obtained, it was concluded that capillary forces play the determining role in the evolution of aggregates and a linear correlaton between the fractal dimensions of aggregates before and after condensation cycle was established. It was shown that the coefficient of proportionality is to a great extent determined by the degree of particle hygroscopicity. A mechanism of change in

¶ We will not dwell on specific features of the mercury porosimetry technique. Detailed information on the subject can be found in, *e.g*., Refs 253 and 254.

the structure of aggregates was proposed [264] and applied to aggregates of carbon black particles in water and benzene vapours. To change the extent of hydrophobicity, the aggregates were exposed to polyethylene glycol vapours. The extent of particle hydrophobicity was monitored by the adsorption isotherms of water vapours. Experiments showed that the change in the aggregate structure strongly depends on the size of condensate droplets. If the droplets were rather large, densification of the entire aggregate occurred to give a dense globule. At small droplet sizes, densification of a small (mainly central) region of the aggregate occurred. A simple model was also proposed in this study, which qualitatively reproduced the experimental dependences.

As mentioned above, capillary forces also change the structure of aggregates in the absence of condensate. Densification of carbon black aggregates on short-term heating to 300 °C [265, 266] and of silica aggregates on prolonged storage [267] was observed. However, in the latter case the mechanism of densification is still to be clarified (formally, the Ostvald ageing and sintering of particles were assumed). The change in the fractal dimension of carbon black particles on heating was also reported.[268] A detailed experimental study on the effect of heating on the fractal characteristics of silver particles was carried out.[269] Aggregates of particles were heated in an inert gas stream over different periods of time at temperatures between 25 and 520 °C. A good correlation between the heating time, temperature and the fractal dimension of aggregates was established (Fig. 5). Based on the results obtained, the possibility of targeted change in the fractal dimension of aggregates of silver particles by varying the temperature and heating time was suggested. The experimental data were in good agreement with the results of Monte Carlo simulation of the sintering of fractal aggregates.[270]

It should be noted that sintering of fractal aggregates is not necessarily accompanied by an increase in their fractal dimension. For instance, it was shown [271] that sintering of rather large fractal aggregates affects the lower and upper cutoff lengths only, whereas the fractal dimension of aggregates remains virtually unchanged. Experiments [272] with silica aerogels confirmed these theoretical results. More detailed models for sintering of aerogels, which predict a constant fractal dimension, were also proposed.[273–275] A detailed study on the laws of changes in the fractal dimension of sintered aggregates was carried out.[276] Using numerical experiments, the relation between the aggregate size and the evolution of its fractal dimension was followed. At small sizes, sintering is unavoidably accompanied by an increase in the fractal dimension. As the aggregate size increases, changes in the fractal dimension become progressively less pronounced in spite of essential changes in the aggregate morphologies.

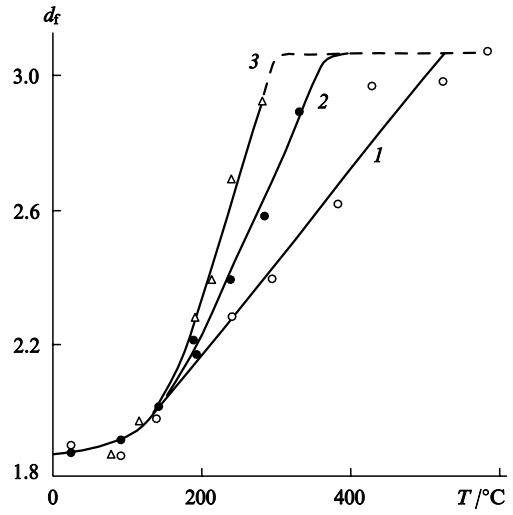


Figure 5. Fractal dimension of silver aggregates plotted *vs.* heating temperature.[269]
Heating time/ s: 1.6 (*1*), 3.2 (*2*) and 4.8 (*3*).

A thermodynamic analysis [277] of sintering of fractal aggregates involved establishment of conditions under which densification of the aggregate structure begins. The possibility of fragmentation of aggregates was also revealed. The calculated temperature dependences of the fractal dimension of gold aggregates coincided with the experimental data.

Numerical simulation of sintering of two-dimensional fractal aggregates due to particle diffusion along the perimeter was carried out [278] using the known aggregation procedure [279] that allows structures with prescribed fractal dimension to be grown. Fragmentation of fractal aggregates was also simulated. The number of fragments was shown to be proportional to the initial surface area of the aggregate. The coefficient of proportionality was a complex function of the fractal dimension of the aggregate (it is only known that this coefficient decreases as d_f increases).

VI. The fractal surface

Many materials, from classical adsorbents to ore particles, have fractal surfaces.[280] In this Section, we will consider the fractal surfaces of porous bodies except for aerogels because of specific morphological features of their surfaces.

The fractal dimension of a surface can be determined using different methods. These are measurements of the surface area using molecules of different size, the micrographs of the cross-sections of porous bodies, the dependence of the surface area of porous particles on their sizes, the time taken to transfer the excitation energy from donor molecules to the adsorbed acceptor molecules, the small-angle X-ray scattering and adsorption measurements, the hydrodynamic permeability of porous bodies, the rates of surface chemical reactions, the kinetics of adsorption, *etc.*[281–283] Many of these methods are based on the description of the kinetics of processes proceeding on fractal surfaces, which requires introduction of new concepts and dimensions. Because of this, we will restrict ourselves to analysis of the classical methods of determination of the fractal dimension of the surface and point out some new approaches. There are a few studies concerned with the development of various models of porous bodies (see, *e.g.*, Refs 284 and 285) and they have much in common with the models employed for the description of growth of fractal aggregates.

The fractal dimension of porous bodies can be determined in a different manner; however, we will not dwell on all of them. Here, mention may be made that the procedure recommended [286] by the IUPAC involves the determination of the fractal dimension of a porous body from the pore size distribution

$$\frac{\mathrm{d}V_\mathrm{p}}{\mathrm{d}r_\mathrm{p}} \propto r_\mathrm{p}^{2-d_\mathrm{f}}\,, \tag{58}$$

where V_p and r_p are the pore volume and pore size, respectively.

1. Small-angle X-ray scattering

Small-angle X-ray and neutron scattering have long been used for the determination of the structure of porous bodies. These methods are suitable for studies on the length scales from atomic sizes to those observed using conventional optical microscopy. This scale range covers virtually all known porous media, being a prerequisite for a wide use of these experimental techniques. The dependence of the scattered intensity, $I(q)$, on the scattering angle (vector), q, is determined by the structure of the porous body.

X-Ray scattering occurs by collisions with electrons while neutron scattering occurs by collisions with atomic nuclei. The scattering by atomic nuclei is governed by the isotope composition of the nuclei. Using various combinations of isotopes, it is possible to enhance or mask certain properties intrinsic in the structure of

the porous body. No significant differences between the results obtained by neutron and X-ray scattering were established.

Peculiar features of the atomic structure do not manifest themselves in the case of small-angle scattering. Because of this, the scattering curves are usually analysed using the two-phase model of a porous body, which assumes that the porous body comprises two phases of constant density, a solid and a void. The intensity of scattering by the fractal surface is given by [287]

$$I(q) = \pi c(\Delta\rho)^2 I_e \Gamma(5-d_f)\sin\left[\frac{\pi(d_f-1)}{2}\right] q^{-(6-d_f)}, \quad (59)$$

where c is a constant, $\Delta\rho$ is the electron density difference (or the neutron scattering length difference) between two phases, I_e is the intensity of scattering by single electron (or by one scatterer) and $\Gamma(x)$ is the gamma function.

At small q, the fractal dimension is determined from the slope of logarithm of the scattered intensity plotted *vs*. logarithm of the scattering angle.

At $d_f = 2$, expression (59) represents the well-known Porod law for X-ray scattering by smooth surfaces,[288, 289] according to which

$$I(q) \propto q^{-4}. \quad (60)$$

This relationship was extended [290] to the case for emission wavelengths comparable with the radius of curvature of smooth surfaces and the corresponding corrections to the Porod law were derived. Yet another expression for the scattered intensity with inclusion of the surface curvature corrections has the form [291]

$$I(q) \propto q^{d_f-6} + q^{d_f-8}\,\frac{(6-d_f)(5-d_f)}{12} \times \left[\frac{1}{R_1R_2} + \frac{3}{8}\left(\frac{1}{R_1}-\frac{1}{R_2}\right)^2\right], \quad (61)$$

where R_1 and R_2 are the principal radii of curvature averaged over the inner (fractal) surface. This relationship was used to determine the fractal dimension of typical adsorbents and the necessity of allowance for the surface curvature corrections in the case of porous bodies was confirmed.

2. Adsorption technique

On length scales shorter than 1 nm the fractal dimension of a surface can be determined by measuring the adsorption capacities of monolayers of molecules of different size δ, and comparing them with the dependence of the surface area on δ

$$\Sigma(\delta) \propto \left(\frac{1}{\delta}\right)^{d_f-2}. \quad (62)$$

The method of determination of the fractal dimension based on evaluation of the surface area according to Brunauer–Emmett–Teller using molecules of different size is often objectionable.[292] This is due to the fact that the surface sites of particular molecules are not known with certainty. As a result, different authors report contradictory data on the fractal dimensions of the same materials, including the values exceeding the limiting d_f value ($d_f = 3$). It should be noted that in some cases one fractal dimension can appear to be insufficient for complete characterisation of the fractal structure of the surface of adsorbents with a complex structure of the pore space. Therefore, one should introduce a hierarchy of fractal dimensions for a given porous body,[293] which can be treated as a particular characteristic of inhomogeneity of the porous body. Introduction of the hierarchy of fractal dimensions corresponds to the so-called multifractal approach (see Section IV in Ref. 1).

On length scales from 1 to 100 nm the fractal dimension is determined from polymolecular adsorption data using two methods. The first is based on the dependence reported by Pfeifer *et al.*[294] (the number of molecules necessary to cover the free surface of the adsorption layer decreases as the layer thickness increases). In the case of adsorption on fractal surfaces, a modified Frenkel–Halsey–Hill equation is used

$$\ln\left(\frac{p}{p_0}\right) = -\frac{A_F}{kT\Gamma^n}, \quad (63)$$

where p is the pressure of the adsorbing gas, p_0 is the saturation pressure, A_F is the parameter determining the adsorbate–adsorbent molecular interaction and Γ is the number of moles of the adsorbed gas. Ignoring the surface tension effects, one gets

$$n = \frac{3}{3-d_f}.$$

If the contribution of surface tension predominates,[295, 296] then

$$n = \frac{1}{3-d_f}.$$

These relationships are valid for self-similar surfaces. In the case of self-affine surfaces, of great importance is the roughness index (α) determining the relation between the surface 'width,' w, and the lateral size, L, of the surface

$$w \propto L^{\alpha}.$$

If the surface tension effects are weak, $n = 3$; if they predominate, $n = 2/\alpha - 1$ at $\alpha > 0.5$ and $n = 3$ at $\alpha < 0.5$ (see Ref. 297).

The Frenkel–Halsey–Hill equation was used by different authors to estimate the fractal dimensions of various porous bodies.[298–300] Recently, the fractal dimension of the surface of adsorbents has been determined using the Dubinin–Astakhov equation generalised to the case for fractal surfaces.[301–303] The Neimark method [304–306] (see above) is also often used to this end.

The fractal dimensions determined using the methods mentioned above were compared in the framework of model calculations.[307] The emphasis was placed on the inclusion of the effect of finite scale range of surface fractality. According to calculations, the fractal dimensions determined using different methods are equal to one another if the range of scales covers two orders of magnitude and can differ by more than 10% if it does not exceed an order of magnitude. This conclusion was confirmed [308] by measuring the fractal dimensions of titania aerogels prepared under different conditions. It was shown that the monolayer and polymolecular adsorption techniques give similar results, though the corresponding fractal dimensions can differ by nearly 0.1. An analogous conclusion was drawn [309] from comparison of the results obtained using different methods in the experiments with silica particles prepared by hydrolysis of tetraethoxysilane in microemulsions. Even the fractal dimensions determined using different methodologies [255, 260] appeared to be similar, though the earlier studies sometimes revealed distinctions between the results obtained by these methods.

Yet another method of determination of the fractal dimensions of porous bodies from the adsorption data was developed by Olivier and co-workers.[310–312] The approach involves construction of the so-called composite adsorption isotherm assuming independent adsorption in pores of each size. For pores of a particular size, the adsorption isotherm is calculated by employing density functional theory.[311] On these assumptions and on imposing the fractal structure of the surface it is possible to construct a composite isotherm whose shape is determined by the fractal dimension of the surface. Comparison of the experimental and model isotherms allows the fractal dimension of the porous medium to be determined. The fractal dimensions of some objects determined using the composite adsorption isotherm were compared [312] with the fractal dimensions estimated using the Frenkel–Halsey–Hill and Neimark equations. It was shown that the fractal dimensions determined using different methods are related by a linear dependences with different slopes (they are determined

by the pore size scales on which the surface exhibits fractal properties).

Yet another reason for significantly different results obtained for different adsorbents using different methods is that porous bodies are characterised by some hierarchy of fractal dimensions rather than a single fractal dimension value (see above). The distribution of fractal dimensions can be rather broad and usually covers the values determined in single experiments.[303]

Two important features should be pointed out. The lower limit of the scale range of surface fractality can be found [304] by comparing the adsorption isotherm for a given sample and the standard adsorption isotherm for the smooth surface. (Strictly speaking, Neimark and Unger [304] reported the upper limit of the scale range of surface fractality.) At the same time, the method proposed provides no possibility for the surface fractality to be established unambiguously and requires additional studies.

The fractal structure of the surface governs the shape of the adsorption isotherms. This is due to the fact that the fractal nature of the substrate affects the properties of the adsorption layer.[313, 314] In particular, it was shown [315] that the inclusion of adsorbent surface fractality allows the Temkin adsorption isotherm to be obtained in the case of non-interacting adsorbate molecules. It was also assumed that wide use of the Temkin isotherm can be explained by frequent occurrence of adsorbents with fractal surfaces.

3. Surface profiles

The adsorption technique is usually employed in studies of the closed fractal surfaces. The fractal dimension of an open surface can be determined by measuring the surface profiles (a single profile for isotropic surface). In the case of anisotropic surfaces, one cross-section is insufficient. There are several methods of processing the surface profile. In particular, it is possible to obtain the height (h_f) correlation function using the relationship

$$R_s(y) = \langle h_f(x) h_f(x+y) \rangle, \tag{64}$$

or to determine the structure function

$$S_s(y) = \langle [h_f(x) - h_f(x+y)]^2 \rangle, \tag{65}$$

where x and $x + y$ are the coordinates in the xy plane.

For fractal surfaces, both the height correlation function and the structural function are related to y by a power-law dependence

$$S_s(y) \propto R_s(y) \propto y^{6-2d_f}.$$

The possibilities of determining the dimensions of the open fractal surfaces using scanning probe microscopy data and surface profile measurements were analysed in detail.[316] It was shown that the shape of the correlation or structural function permits not only the fractal dimension to be determined but also the characteristic length scale of surface fractality to be revealed in the case of self-affine surfaces.

Going to longer length scales exceeding the upper limit of surface fractality does not mean [317] a constant surface area measured by probes of different size. Even on long length scales, the surface area measured depends on the probe size because it becomes rough due to fluctuations. In this case, the surface area measured decreases obeying a power law as the probe size increases,[317] the exponent being dependent on the fractal dimension in a much more complex manner compared to relation (62).

Peculiarities of the behaviour of the structure and correlation functions as well as problems that arise in determining the fractal dimension of anisotropic surfaces were considered in detail by Wu.[318, 319] In particular, it was shown that the fractal dimensions of model surfaces can depend on the type of the function (S_s or R_s) employed in the computational procedure. The fractal dimension can also be a function of other physicochemical parameters of solids.[320]

4. Other methods

An original method [321] of determination of the fractal dimension of metallic surfaces involves scattering studies of surface plasmon polaritons (SPP) by rough surfaces. In the case of well-developed fractal surface, localisation of the SPP is possible. The scheme of calculations of the fractal dimension using the laws of SPP scattering was evaluated taking films grown by evaporation–condensation in different regimes suitable for preparation of smooth and rough surfaces. The fractal dimensions determined are in good agreement with those found using the film surface profiles.

The fractal dimensions of the surfaces of conducting solids can be determined using electrochemical methods. Comparison of the fractal dimensions determined using atomic force microscopy and cyclic voltammograms appeared to be similar.[322]

The method proposed [323] for semiconductor films involves measurements of the photocurrent from their surface. It was assumed that the photocurrent (I_f) is proportional to the absorbed energy and, correspondingly, to the surface area of the specimen. In this case

$$I_f \sim L^{d_f}, \tag{66}$$

where L is the linear dimension of the specimen.

Experiments [323] carried out using films of different linear size gave the fractal dimensions which coincided with those determined for the same films using atomic force microscopy.

Yet another method of determination of the fractal dimensions of the open surfaces was proposed in a study [324] on the laws of scattering of helium atoms by silver submonolayers of different structure on Pt (111). According to calculations, the scattered intensity is related to the difference between the tangential components of the wave vectors of the incident and scattered atomic beams (Δk)

$$I_a(\Delta k) \sim (\Delta k)^{d_f - 4}. \tag{67}$$

This relation was confirmed experimentally. The technique seems to be promising because experimental methods of studies on scattering of atoms and molecules by solid surfaces are well developed.

VII. Aerogels

Aerogels are used as heat insulators, catalyst supports,[325] reservoirs for flammable fluids and elements of acoustical and optical devices,[326] in Cherenkov counters [327] and solar cells,[328] for the growth of photoluminescent silicon crystals [329] (in this case, aerogels themselves can possess photoluminescent properties [330]). Aerogels are highly porous, low density materials characterised by small pore sizes. They are produced by drying hydrogels prepared by a sol–gel process under supercritical conditions. In particular, the most widely used silica aerogels are prepared by hydrolysis of tetraethoxysilane or tetramethoxysilane in aqueous alcoholic solutions. Aerogels of other metal oxides are prepared from corresponding alkoxides.[326]

The sol–gel process involves hydrolysis of precursors followed by polycondensation of hydrolysis products. Particles formed during polycondensation (sol) aggregate and then form a continuous network (gel). Preparation of gel is followed by its drying. Depending on the drying regime, a glass, ceramic or aerogel can be obtained. The density of aerogels can be varied within two orders of magnitude from several hundredth to 1 g cm^{-3}.

Studies of aerogels face some difficulties [331] because of strong perturbations introduced into the structure of aerogels when using conventional methods such as mercury porosimetry, thermoporosimetry and adsorption technique. Therefore, these objects are often studied using contact-free methods, *viz*., small-angle neutron, light and X-ray scattering as well as optical, acoustical and thermomechanical methods.

It has long been established using small-angle X-ray [332, 333] and neutron [334, 335] scattering that aerogels have a fractal structure on the length scales from several to 1000 Å and that their mass fractal dimensions lie between 2.1 and 2.4. The pore surface of aerogels is also fractal; the parameter d_f can approach the limiting value (≈ 3).

The longest length scale, ξ, of aerogel fractality is usually called the correlation length (by analogy with the correlation length in percolation theory). The size of fractal domains is, as a rule, from several tens to a hundred of nanometres. The density of aerogels equals that of the gel-forming fractal clusters and is determined by the correlation length

$$\rho(\xi) = \rho_0 \left(\frac{\xi}{a}\right)^{d_f - 3}, \tag{68}$$

where ρ_0 is the density of the substance the primary particles of radius a are made of. The pore size distribution for aerogels also obeys a power-law dependence.[336]

Consider the results of several recent investigations on the structure of aerogels. Reidy *et al.*[337] reported a small-angle neutron scattering study of the structures of three aerogels prepared by hydrolysis of tetraethoxysilane (TEOS), triethoxysilane (TES) and trimethoxysilane (TMS). Three gel models were employed, the interference, fractal and maximum entropy ones. The first model assumes that aerogel is composed of homogeneous spheroidal granules with a prescribed aspect ratio and lognormal size distribution.[338] According to the second model, gel comprises fractal fragments of size ξ. The third model treats gel as a system of homogeneous particles and derives a particle size distribution consistent with the maximum configuration entropy.[339] Analysis of scattering patterns showed that the TEOS aerogels were best described by the maximum entropy model, while the TES and TMS aerogels were best described by the fractal model (a version with fractal primary particles for TES aerogels and with fractal surface of the pore space for TMS aerogels).

The structures of aerogels can be modified in a different manner. The most efficient way is to introduce an aerosil into the disperse medium. This can result in aerogels which either have no fractal structure [340] or have a binary fractal structure.[341] When aerogels were prepared from sodium silicate solutions, the gel structure was strongly dependent [342] on the pH value of the medium, which can be attributed to the change in the surface charge of the primary particles, which governs the rate of coagulation and the fractal dimension of aggregates. The addition of hydrogen peroxide to aerogels prepared by hydrolysis of methyl silicate led to somewhat unexpected results.[343] Namely, the fractal dimension of certain systems remained unchanged and even increased as their density decreased.

The mechanical properties of aerogels are of great practical value and therefore attract particular attention. The power-law dependence of the Young's modulus, E, of aerogels on their density ρ (ρ_0 is the density of the framework-forming material)

$$E = E_0 \left(\frac{\rho}{\rho_0}\right)^m \tag{69}$$

was confirmed in numerous studies. The exponent m is not a universal scaling factor; even for the silica-based gels it varies from 2.5 to 3.8 depending on the substances used for the preparation of aerogels and on the regimes of subsequent drying and heat treatment. Apparently, this exponent is related to the fractal dimension of aerogel; however, this was not rigorously substantiated. A possible relation is as follows:[344]

$$m = \frac{5 - d_f}{3 - d_f}. \tag{70}$$

The mechanical properties of aerogels are often described using the bulk modulus K_b, which relates the change, Δp, in the pressure applied to a sample to the relative change in the sample volume

$$\Delta p = -K_b \left(\frac{\Delta V}{V}\right). \tag{71}$$

The moduli E and K_b are related by

$$K_b = \frac{E}{3(1 - 2\nu)},$$

where ν is the Poisson ratio.

The modulus K_b is also related to the density by a power-law dependence

$$K_b = \rho^{\kappa_b}, \tag{72}$$

where the exponent κ_b for silica aerogel varies from 3.08 to 3.38 (the mean values are ≈ 3.2 and 3.6 in the regions of plastic and elastic deformation, respectively).[345] Analysis of a large array of experimental data on the elastic moduli of aerogels revealed [346] an unambiguous relation between the parameter κ_b and the pore size distribution and a hierarchy of pore size distributions over a broad range of length scales provided that relationship (72) is valid.

At temperatures below 1 K, the specific heat of aerogels obeys the law

$$C_p \sim T^{\alpha_c},$$

where the exponent α_c ($\alpha_c \approx 1.4$) is virtually independent of the density of ultralight aerogels ($\rho < 0.4$).[347] The thermal conductivity of aerogels is a constant at low temperatures and increases in proportion to T^{α_t} ($\alpha_t \approx 1.2$) at higher temperatues. At low temperatures, the specific heat of aerogels is determined by the phonon density of states. Brillouin scattering studies revealed that the frequency dependence, $N_v(\omega)$, of the density of phonon states at the wavelengths comparable with the length scales of domains of the fractal structure of aerogels deviates from the dependence typical of the phonon spectrum. Namely, this dependence still obeys a power law but the exponent changes from $(d-1)$ to $(d_{fr}-1)$

$$N_v(\omega) \sim \omega^{d_{fr}-1}.$$

The new exponent is called a fracton or the spectral dimension. For silica aerogels, $d_{fr} \approx 1.3$. The fracton dimension characterises specific features of the oscillations of those aerogel fragments which have a fractal structure. Peculiarities of the vibrational spectra of fractal structures and aerogels have been analysed in detail (see Refs 189 and 348, respectively); therefore, we will not dwell on them. Mention may be made that the fracton concept was first proposed by Alexander and Orbach.[237]

Fractons are natural oscillations of a fractal. If aerogel is treated as a set of fractal clusters, fractons characterise peculiar features of their vibrational dynamics. Strictly speaking, the fracton dimension of clusters 'grown' in numerical experiments can be determined only in analogous numerical simulation (see, *e.g.*, Ref. 349). According to calculations, the fracton dimension weakly depends on the fractal dimension. At the same time, an analytical relation between these dimensions was derived in the framework of a certain model. A simple equation was proposed,[350]

$$d_{fr} = \frac{d_f}{1 + b(3 - d_f)}, \tag{73}$$

in which the parameter b determines the dependence of the velocity of sound, v_s, on the aerogel density

$$v_s(\rho) \propto \rho^b.$$

Relation (73) was reported [351] as a particular case of general relations derived for elastic and thermal characteristics of hierarchic structures. Some other relationships are as follows:

$$b = \frac{m-1}{2}, \tag{74}$$

$$\alpha_t = d_{fr} + \frac{1-2d_{fr}}{d_f},$$

$$\alpha_c = d_{fr}.$$

In addition to Brillouin scattering, the Raman light scattering also plays a significant role in studies of aerogels. It was shown [352] that the response of the Raman scattering by aerogels depends on the frequency of electromagnetic radiation (ω) and is described by a universal law

$$\chi_R(\omega) \sim \omega^{-\phi}, \tag{75}$$

where the exponent ϕ is determined by three dimensions, *viz*., the mass fractal dimension, d_f; the fracton dimension, d_{fr}, which characterises the density of vibrational states; and the dimension d_σ characterising the deformation of particles by fractons. The dependence of the exponent ϕ on these dimensions is determined by the mechanism of Raman scattering. If the mechanism involves the interaction between permanent and induced dipoles, then

$$\phi_{dd} = 2\left[\frac{d_{fr}}{d_f}(d_f - 3 - d_\sigma)\right] + 1. \tag{76}$$

If the mechanism involves modulation of the polarisability by atomic oscillations, one has

$$\phi_p = 2\left(1 - \frac{d_{fr}d_\sigma}{d_f}\right). \tag{77}$$

Relationships (75)–(77) were verified taking silica aerogels of different density as examples.[353] Gels were heat treated and exposed to hydrostatic load and uniaxial compression. Experiments with all samples showed that the parameter ϕ is independent of the density of gel and remains unchanged during heat treatment of aerogels resulting in their densification. However, mechanical deformation favoured a decrease in ϕ due to a change in the fracton dimension of the loaded samples.

Changes in other mechanical and fractal characteristics of aerogels due to their densification were also studied.[354–356] Structural changes were mainly detected using small-angle X-ray scattering. Densification of aerogels caused the correlation length to decrease, while the fractal dimension slightly increased (Fig. 6). As a rule, the corresponding parameters of the densified aerogels and of the initially more dense aerogels coincided. In some cases the fractal dimension of the mechanically compressed aerogels remained unchanged.[356]

More significant were the changes in the fractal dimension upon densification by sintering.[357–359] Analysis showed [271, 274, 360, 361] that, in spite of an increase in the fractal dimension of aerogels on sintering, a great body of information on the initial structure is retained. The difference between mechanical compression and sintering consists in that sintering causes densification of the network of bonds while mechanical compression causes restructuring of aggregates without formation of new bonds. Noteworthy is that the changes in the structure of aerogels on compression or sintering implicitly affect their physicochemical properties. For instance, it was shown both theoretically [362] and experimentally [363] that the gas permeability of aerogels depends solely on their density which can vary over a wide range.

Aerogels have a fractal pore surface.[308, 330, 364–370] The fractal dimension can be determined by various methods and usually lies between 2.5 and 2.8, though in some cases can reach the limiting values 2.92–2.98 (see Refs 308 and 364). The fractal dimension of the surface of aerogels strongly depends on the procedure employed for the preparation of gel (more exactly, on the regimes of drying,[365–368] ageing [369] and mechanical treatment.[370]) Heat treatment of aerogels usually causes the fractal dimensions of their surfaces to decrease, while mechanical treatment can cause both a decrease and an increase in d_f.[370]

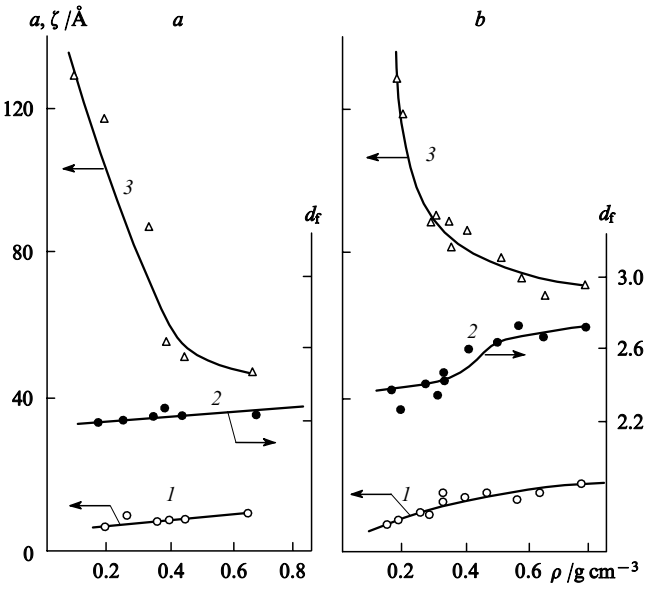


Figure 6. The size of primary particles (*1*), the fractal dimension (*2*) and the correlation length (*3*) plotted *vs*. the bulk density for mechanical densification (*a*) and sintering (*b*) of aerogels.[356]

No rigorous correlation between the bulk fractal dimension of aerogels and the fractal dimension of their surfaces was established as yet. Even an increase in the bulk fractal dimension was observed [369] in the experiments on ageing of aerogels accompanied by a dramatic decrease in the fractal dimension of the surface from 2.75 down to a value of 2, which is typical of a non-fractal surface.

VIII. Conclusion

The methods of fractal geometry are widely used in natural science. As shown by the material presented in this review and in Ref. 1, intensive research on the fractal structures is being carried out. Because of the extensive literature on the subject, many aspects of physical chemistry of the surface phenomena and colloidal systems are left out of consideration. We can only give a short list of the most important research avenues. The fractal approach is employed in the studies on the properties of foams [371, 372] and on the kinetics of binding of bioactive molecules with surface-immobilised receptors.[373–378] The fractal analysis is used to describe replacement of nucleotides in DNA molecules [379] and to analyse spontaneous aggregation of multilayered lipid vesicles.[380] Recently, considerable attention has been paid to fractal aggregates growing in sea water.[381, 382] Sedimentary rocks also have fractal surfaces.[383–385] The fractal structure of cracks developing in brittle materials and polymers [386–388] is described using not only the conventional fractal approach but also multifractal methodology.[389, 390] The behaviour of grain boundaries in polycrystalline materials [391] and their transformations on exposure to various external factors [392] is considered in the framework of fractal formalism. Reversal of the magnetisation of thin polycrystalline layers is treated [393] as a development of fractal clusters composed of magnetic domains. Fractal concepts are used in studies on capillary electrophoresis [394] and simulation of growth of gallstones.[395] This list of research avenues that successfully employ the concepts of growth of fractal structures is far short from being complete.

In spite of extensive literature concerning the fractal structures in various colloidal systems, many problems are still to be solved. The totality of experience accumulated during the last two decades shows that often solving new applied problems requires revision of the foundations of theory of fractal objects. Therefore, the development of fractal concepts is inevitable.

References

1. V I Roldughin *Usp. Khim.* **72** 931 (2003) [*Russ. Chem. Rev.* **72** 823 (2003)]
2. D A Weitz, M Oliveria *Phys. Rev. Lett.* **52** 1433 (1984)
3. D A Weitz, J S Huang, M Y Lin J Sung *Phys. Rev. Lett.* **54** 1416 (1985)
4. M Tence, J R Chevalier, R Jullien *J. Phys. (France)* **47** 1989 (1986)
5. J Cai, N Lu, C M Sorensen *J. Colloid Interface Sci.* **171** 470 (1995)
6. J Cai, N Lu, C M Sorensen *Langmuir* **9** 2861 (1993)
7. B M Smirnov *Fizika Fraktal'nykh Klasterov* (The Physics of Fractal Clusters) (Moscow: Nauka, 1991)
8. M Yu Yablokov *Zh. Fiz. Khim.* **73** 214 (1999) [a]
9. M Miyazima, H E Stanley *Phys. Rev. B* **35** 8898 (1987)
10. F Zaratarian, C Mustin, G Villemin, T Ait-Ettager, A Thill, J Y Bottero, J L Mallet, D Snidaro *Langmuir* **13** 35 (1997)
11. A Thill, M Wagner, J Y Bottero *J. Colloid Interface Sci.* **220** 465 (1999)
12. P Dimon, S K Sinha, D A Weitz, C R Safinya, G S Smith, W A Varady, H M Lindsay *Phys. Rev. Lett.* **57** 595 (1986)
13. D W Schaefer, K D Keefer *Phys. Rev. Lett.* **56** 2199 (1986)
14. M A V Axelos, D Tchoubar, R Jullien *J. Phys. (France)* **47** 1843 (1986)
15. D W Schaefer, B J Olivier, A J Hurd, G B Beaucage, J J Ivie, C R Herd *J. Aerosol Sci.* **22** (Suppl. 1) S447 (1991)
16. A Hasmy, M Foret, J Pelous, R Jullien *Phys. Rev. B* **48** 9345 (1993)
17. S H Chen, J Teixeira *Phys. Rev. Lett.* **57** 2583 (1986)
18. K Wong, B Cabane, R Duplessix *J. Colloid Interface Sci.* **123** 466 (1988)
19. G C Bushell, R Amal, J A Paper *Physica A* **233** 859 (1996)
20. C M Sorensen, J Cai, N Lu *Appl. Opt.* **31** 6547 (1992)
21. C Aubert, D S Cannell *Phys. Rev. Lett.* **56** 738 (1986)
22. J E Martin, A J Hurd *J. Appl. Crystallogr.* **20** 61 (1987)
23. Z Zhou, P Wu, B Chu *J. Colloid Interface Sci.* **146** 541 (1991)
24. V Oles *J. Colloid Interface Sci.* **154** 351 (1992)
25. R Amal, J A Paper, T D Waite *J. Colloid Interface Sci.* **140** 158 (1990)
26. J E Martin, J P Wilcoxon, D Schaefer, J Odinek *Phys. Rev. A* **41** 4379 (1990)
27. B J Olivier, C M Sorencen *J. Colloid Interface Sci.* **134** 139 (1990)
28. D A Weitz, J S Huang, M Y Lin, J Sung *Phys. Rev. Lett.* **53** 1657 (1984)
29. M Y Lin, H M Lindsay, D A Weitz, R C Ball, R Klein, P Meakin *Proc. R. Soc., London, Ser. A* **423** 71 (1989)
30. M Y Lin, H M Lindsay, D A Weitz, R C Ball, R Klein, P Meakin *Phys. Rev. A* **41** 2005 (1990)
31. M Y Lin, H M Lindsay, D A Weitz, R Klein, R C Ball, P Meakin *J. Phys.: Condens. Matter* **2** 3093 (1990)
32. M Carpineti, F Ferri, M Giglio, E Paganini, U Perini *Phys. Rev. A* **42** 7347 (1990)
33. D Asnaghi, M Carpineti, M Giglio, M Sozzi *Phys. Rev. A* **45** 1018 (1992)
34. M V Lin, R Klein, H M Lindsay, D A Weitz, R C Ball, P Meakin *J. Colloid Interface Sci.* **137** 263 (1990)
35. N G Khlebtsov, A G Mel'nikov *Kolloidn. Zh.* **55** 167 (1993) [b]
36. R Ch Bokun *J. Aerosol Sci.* **26** (Suppl. 1) 933 (1995)
37. N G Khlebtsov *Kolloidn. Zh.* **58** 100 (1996) [b]
38. P W Zhu, J W White *J. Chem. Phys.* **104** 9169 (1996)
39. T Nicolai, D Durand, J-C Gimel *Phys. Rev. B* **50** 16357 (1994)
40. B R Berne, R Pecora *Dynamic Light Scattering* (New York: Wiley-Interscience, 1976)
41. M Shibayama, T Norisuye *Bull. Chem. Soc. Jpn.* **75** 641 (2002)
42. N Terao, T Nakayama *Prog. Theor. Phys.* **138** 354 (2000)
43. M Carpineti, M Giglio *Phys. Rev. Lett.* **70** 3828 (1993)
44. D Asanaghi, M Carpineti, M Giglio, A Vailati *Physica A* **213** 148 (1995)
45. A Hasmy, E Anglaret, M Foret, J Pelous, R Jullien *Phys. Rev. B* **50** 6006 (1994)
46. B J Olivier, C M Sorensen *Phys. Rev. A* **41** 2093 (1990)
47. X Jiang, G Chen *J. Chem. Ind. Eng.* **50** 337 (1999)
48. A S Kyriakidis, A G Yiantsosis, A J Karabelas *J. Colloid Interface Sci.* **195** 299 (1997)
49. Y H Rim, J D Cawley *Ceram. Trans.* **26** 54 (1992)
50. A Y Kim, J C Berg *J. Colloid Interface Sci.* **229** 607 (2000)
51. J Chorover, J Zhang, M K Amistadi, J Buffle *Clays Clay Miner.* **45** 690 (1997)
52. T D Wait, J K Cleaver, J K Beattie *J. Colloid Interface Sci.* **241** 333 (2001)
53. G Vigil, Z Xu, S Steinberg, J Israelachvili *J. Colloid Interface Sci.* **165** 367 (1994)
54. M P B Van Bruggen, M Donker, H N W Lekkerkerker, T L Hughes *Colloids Surf.* **150** 115 (1999)
55. M E Karman, R M Pashley, T D Waite, S J Hatch, H Bustamante *Colloids Surf.* **129–130** 239 (1997)
56. J Lui, W Y Shih, M Sarikaya, I A Aksay *Phys. Rev. A* **41** 3206 (1990)
57. W Y Shin, I I Aksay, R Kikuchi *Phys. Rev. A* **36** 5015 (1987)
58. P Bezot, C Hesse-Bezot, C Diraison *Carbon* **35** 53 (1997)
59. M V Shamurina, V I Roldughin, T D Pryamova, V V Vysotskii *Kolloidn. Zh.* **57** 580 (1995) [b]
60. P W Zhu, D H Napper *Phys. Rev. E* **50** 1360 (1994)
61. M Tirado-Miranda, A Schmitt, J Callejas-Fernandez, A Fernandez-Barbero *Langmuir* **15** 3437 (1999)
62. R Ferretti, J Zhang, J Buffle *J. Colloid Interface Sci.* **208** 509 (1998)
63. R Amal, J A Raper, T D Waite *J. Colloid Interface Sci.* **151** 244 (1992)
64. M Thies, U Hinze, H H Paradies *Ber. Bunsen-Ges. Phys. Chem.* **100** 501 (1996)
65. J Zhang, J Buffe *J. Colloid Interface Sci.* **174** 500 (1995)
66. R Ferretti, J Zhang, J Buffe *Colloids Surf. A* **121** 203 (1997)
67. R Jullien, R Botet, P M Mors *Discuss. Faraday Soc.* **83** 125 (1987)
68. R Jullien, P Meakin *J. Colloid Interface Sci.* **127** 265 (1989)
69. P Meakin *J. Colloid Interface Sci.* **112** 187 (1986)
70. R T C Ju, C W Frank, A P Gast *Langmuir* **8** 2165 (1992)
71. J A Molina-Bolivar, F Galisteo-Gonzalez, R Hidalgo-Alvarez *J. Colloid Interface Sci.* **208** 445 (1998)
72. S Guillot, D Lairez, M A V Axelos *J. Appl. Crystallogr.* **33** 669 (2000)
73. S Nyeki, I Colbeck *J. Aerosol Sci.* **25** 75 (1994)
74. S Nyeki, I Colbek *Aerosol Sci. Technol.* **127** 109 (1995)
75. H M Lindsay, R Klein, D A Weitz, M Y Lin, P Meakin *Phys. Rev. A* **39** 3112 (1989)
76. M V Shamurina, V I Roldughin, T D Pryamova, V V Vysotskii *Kolloidn. Zh.* **56** 451 (1994) [b]
77. Ü Ö Köylü, Y Xing, D E Rosner *Langmuir* **11** 4848 (1995)
78. A V Neimark, Ü Ö Köylü, D E Rosner *J. Colloid Interface Sci.* **180** 590 (1996)
79. K Starchev, S Stoylov *Phys. Rev. B* **47** 11725 (1993)
80. K Starchev, I Petkanchin, S Stoylov *Langmuir* **10** 1456 (1994)
81. N G Khlebtsov, A G Mel'nikov, V A Bogatyrev *Kolloidn. Zh.* **59** 691 (1997) [b]
82. N G Khlebtsov, A G Mel'nikov *Kolloidn. Zh.* **60** 843 (1998) [b]
83. N G Khlebtsov, V A Bogatyrev, A G Melnikov, A I Sirota *J. Quant. Spectrosc. Radiat. Transf.* **63** 469 (1999)
84. N G Khlebtsov, V A Bogatyrev *Kolloidn. Zh.* **63** 528 (2001) [b]
85. F Mantegazza, M E Giardini, V Degiorgio, D Asnaghi, M Gilgio *J. Colloid Interface Sci.* **170** 50 (1995)
86. V I Roldughin, D V Voronin *Kolloidn. Zh.* **63** 394 (2001) [b]
87. A E Gonzales *Phys. Rev. Lett.* **71** 2248 (1993)
88. A Di Biasio, G Bolle, C Cametti, P Codastefano, F Sciortino, P Tartaglia *Phys. Rev. E* **50** 1649 (1994)
89. G Odriozola, M Tirado-Miranda, A Schmitt, F Martinez-Lopez, J Callejas-Fernandez, R Martinez-Garcia, R Hidalgo-Alvarez *J. Colloid Interface Sci.* **240** 90 (2001)
90. A Y Kim, J C Berg *Langmuir* **16** 2101 (2000)
91. M Carpineti, M Giglio *J. Phys.: Condens. Matter* **6** A329 (1993)
92. S D T Axford *J. Chem Soc., Faraday Trans.* **93** 303 (1997)
93. M Carpineti, M Giglio *Phys. Rev. Lett.* **68** 3327 (1992)

94. A Schmitt, G Odriozola, A Moncho-Jorda, J Callejas-Fernandez, R Martinez-Garia, R Hidalgo-Alvarez *Phys. Rev. E* **62** 8335 (2000)
95. M Katzer, A P Weber, G Kasper *J. Colloid Interface Sci.* **240** 67 (2001)
96. S N Rogak, U Baltensperger, R C Flagan *Aerosol Sci. Technol.* **14** 447 (1991)
97. S N Rogak, U Baltensperger, S E Pratsinis *Aerosol Sci. Technol.* **14** 514 (1991)
98. W Haas, M Zrinyi, H-G Killan, B Heise *Colloid Polym. Sci.* **271** 1024 (1993)
99. M Zrinyi, M Kabai-Faix, Sz Juhos, F Horkay *Langmuir* **9** 71 (1993)
100. R Brunner S Gall, W Wilke, M Zrinyi *Physica A* **214** 153 (1995)
101. P Meakin, Z-Y Chen, P Evesque *J. Chem. Phys.* **87** 630 (1987)
102. A P Philipse, A M Wierenga *Langmuir* **14** 49 (1998)
103. A Vailati, D Asnaghi, M Giglio, R Piazza *Phys. Rev. E* **48** R2358 (1993)
104. V Degiordio, R Piazza, T Bellini, M Visca *Adv. Colloid Interface Sci.* **48** 61 (1994)
105. G Bushell, R Amal *J. Colloid Interface Sci.* **221** 186 (2000)
106. C Xiong, S K Friedlander *Proc. Natl. Acad. Sci. USA* **98** 11 851 (2001)
107. F Mallamace, N Micali, S Trusso, L M Scolaro, A Romeo, A Terracina, R F Pasternak *Phys. Rev Lett.* **76** 4741 (1996)
108. S Z Ren, E Tombacz, J A Rice *Phys. Rev. E* **53** 2980 (1996)
109. G Skillas, H Burtscher, K Siegmann, U Baltensperger *J. Colloid Interface Sci.* **217** 269 (1999)
110. T Rudalevige, A H Francis, R Zand *J. Phys. Chem. B* **102** 9797 (1998)
111. E T Kisak, M T Kennedy, D Trommeshauser, J A Zasadzinski *Langmuir* **16** 2825 (2000)
112. M Sano, K Onishi, T Ishii, S Shinkai *Langmuir* **16** 3773 (2000)
113. B Lo, D Wait *J. Colloid Interface Sci.* **222** 83 (2000)
114. T Nicula *Indian J. Phys. B* **72** 631 (1998)
115. S Wang, H Xin *J. Phys. Chem. B* **104** 5681 (2000)
116. H-G Zhang, F-Z Liu, T-J He, H-W Xin *Sci. China, B* **37** 395 (1994)
117. P Meakin, Z-Y Chen, J M Deutsch *J. Chem. Phys.* **82** 3768 (1985)
118. W Hess, H L Frisch, R Klein *Z. Phys. B: Condens. Matter* **64** 65 (1986)
119. S N Rogak, R C Flagan *J. Colloid Interface Sci.* **134** 206 (1990)
120. S Veerapaneni, M R Wiesner *J. Colloid Interface Sci.* **117** 45 (1996)
121. Z Chen, P Meakin, J M Deutch *Phys. Rev. Lett.* **59** 2121 (1987)
122. P N Pusey, J G Rarity, R Klein, D A Weitz *Phys. Rev. Lett.* **59** 2122 (1987)
123. P Wiltzius *Phys. Rev. Lett.* **58** 710 (1987)
124. W Van Saarloos *Physica A* **147** 280 (1987)
125. J G Kirkwood, J Riseman *J. Chem. Phys.* **16** 565 (1948)
126. L Gmachowski *J. Colloid Interface Sci.* **178** 80 (1996)
127. M Vanni *Chem. Eng. Sci.* **55** 685 (2000)
128. A L Chernyakov *Zh. Eksp. Teor. Fiz.* **120** 883 (2001) [c]
129. A V Filippov *J. Colloid Intrface Sci.* **229** 184 (2000)
130. A V Filippov *J. Colloid Interface Sci.* **241** 479 (2001)
131. A V Filippov, M Zurita, D E Rosner *J. Colloid Interface Sci.* **229** 261 (2000)
132. X-Y Li, B E Logan *Water Res.* **14** 3373 (2001)
133. R Hagenloch, S K Friedlander *J. Colloid Interface Sci.* **133** 185 (1989)
134. P Meakin, B Donn, G W Mulholland *Langmuir* **5** 510 (1989)
135. V V Uchaikin, D A Korobko *Pis'ma Zh. Tekhn. Fiz.* **25** 34 (1991) [d]
136. R C Sonntag, W C Russel *J. Colloid Interface Sci.* **113** 111 (1986)
137. R C Sonntag, W C Russel *J. Colloid Interface Sci.* **115** 378 (1987)
138. R Wessel, R C Ball *Phys. Rev. A* **46** R3008 (1992)
139. Y Kantor, I Webman *Phys. Rev. Lett.* **52** 1891 (1984)
140. Y Kantor, T A Witten *J. Phys. Lett.* **45** L675 (1984)
141. P Meakin, J M Deutch *J. Chem. Phys.* **86** 4648 (1987)
142. M Blunt *Phys. Rev. A* **39** 5801 (1989)
143. A Potanin *J. Chem. Phys.* **96** 9191 (1992)
144. A Potanin *J. Colloid Interface Sci.* **157** 399 (1993)
145. A A Potanin, V M Muller *Kolloidn. Zh.* **57** 553 (1995) [b]
146. M Chen, W B Russel *J. Colloid Interface Sci.* **141** 564 (1991)
147. M Doi, D Chen *J. Chem. Phys.* **90** 5271 (1989)
148. M Doi, D Chen *J. Chem. Phys.* **91** 2656 (1990)
149. S B Santra, H J Herrmann *Physica A* **218** 298 (1995)
150. P B Warren, R C Ball, A Boelle *Europhys. Lett.* **29** 339 (1995)
151. T Kovacs, G Bardos *Physica A* **247** 59 (1997)
152. A A Potanin *Kolloidn. Zh.* **52** 1101 (1990) [b]
153. F E Torres, W B Russel, W R Schowalter *J. Colloid Interface Sci.* **142** 554 (1991)
154. F E Torres, W B Russel, W R Schowalter *J. Colloid Interface Sci.* **145** 51 (1991)
155. F J Muzzio, J M Ottino *Phys. Rev. A* **38** 2516 (1988)
156. S Hansen, J M Ottio *J. Colloid Interface Sci.* **179** 89 (1996)
157. P Marsh, G Bushell, R Amal *J. Colloid Interface Sci.* **241** 286 (2001)
158. B M Dogonosov *Kolloidn. Zh.* **63** 39 (2001) [b]
159. P T Spicer, W Keller, S E Pratsinis *J. Colloid Interface Sci.* **184** 112 (1996)
160. T Serra, J Colomer, X Casamitjana *J. Colloid Interface Sci.* **187** 466 (1997)
161. T Serra, X Casamitjana *J. Colloid Interface Sci.* **206** 505 (1998)
162. K H Gardner,T L Theis, T C Young *Water Res.* **32** 2660 (1998)
163. C Selomulya, R Amal, G Bushell, T D Wait *J. Colloid Interface Sci.* **236** 67 (2001)
164. S Tang, J M Preece, C M McFarlane, Z Zhang *J. Colloid Interface Sci.* **221** 114 (2000)
165. H Saint-Raymond, F Gruy, M Cornil *J. Colloid Interface Sci.* **186** 447 (1997)
166. F Gruy *J. Colloid Interface Sci.* **237** 28 (2001)
167. C Allain, M Cloitre *Adv. Colloid Interface Sci.* **46** 129 (1993)
168. L L Hoekstra, R Vreeker, W G M Agterot *J. Colloid Interface Sci.* **151** 17 (1992)
169. D G Lee, J S Bonner, L S Garton, A N S Ernest, R L Autenrieth *Water Res.* **34** 1987 (2000)
170. D G Lee, J S Bonner, L S Garton, A N S Ernest, R L Autenrieth *Water Res.* **36** 1056 (2002)
171. P Deladurantaye, C Rioux, R J Slobodrian *Chaos, Solitons, Fractals* **8** 1693 (1997)
172. C Allain, M Cloitre, F Parisse *J. Colloid Interface Sci.* **178** 411 (1996)
173. M Zrinyi, M Kabai-Faix, F Horkay *Prog. Colloid Polym. Sci.* **77** 165 (1988)
174. T Aubry, B Largenton, M Moan *J. Colloid Interface Sci.* **202** 551 (1998)
175. R Buscale *Colloids Surf.* **43** 33 (1990)
176. A V Ignatchenko, G F Smagina, A B Solokhina, O A Besedina, I G Idrisov *Kolloidn. Zh.* **54** 55 (1992) [b]
177. M M Takayasu, F Galembeck *J. Colloid Interface Sci.* **202** 84 (1998)
178. E D Molodtsova, V I Roldughin *Kolloidn. Zh.* **54** 102 (1992) [b]
179. Z Wu, I Colbeck, S Simons *J. Phys. D: Appl. Phys.* **27** 2291 (1994)
180. P Tang, J Greenwood, J A Raper *J. Colloid Interface Sci.* **247** 210 (2002)
181. E F Mikhailov, S S Vlasenko *Khim. Fiz.* **11** 571 (1992) [e]
182. Y Liu, L Gao, L Yu, J Guo *J. Colloid Interface Sci.* **227** 164 (2000)
183. I Ya Ladyzhenskii *Kolloidn. Zh.* **54** 93 (1992) [b]
184. A A Potanin, W B Russel *Phys. Rev. E* **53** 3702 (1996)
185. L Bergström *J. Chem. Soc., Faraday Trans.* **88** 3201 (1992)
186. P A Heiny, R J Butera, J D Londono, R V Davidson, S Mazur *J. Phys. Chem. B* **104** 8807 (2000)
187. S Ikeda, E A Foegeding, T Hagiwara *Langmuir* **15** 8584 (1999)
188. V V Zosimov, L M Lyamshev *Usp. Fiz. Nauk* **165** 361 (1995) [*Physics-Uspekhi* **38** 346 (1995)]
189. A A Potanin, N B Ur'ev *Kolloidn. Zh.* **53** 52 (1991) [b]
190. I Ya Ladyzhenskii, G N Ur'eva, Ya Mevis, N B Ur'ev *Kolloidn. Zh.* **54** 91 (1992) [b]
191. D P Patel, W B Russel *Colloids Surf.* **31** 355 (1988)
192. W H Shih, W Y Shih, S I Kim, J Liu, I A Aksay *Phys. Rev. A* **42** 4772 (1990)
193. A A Potanin *J. Colloid Interface Sci.* **145** 140 (1991)
194. A A Potanin *J. Colloid Interface Sci.* **156** 143 (1993)
195. A A Potanin, R De Rooij, D Van den Ende, J Mellema *J. Chem. Phys.* **102** 5845 (1995)
196. M Whittle, E Dickinson *J. Chem. Phys.* **107** 10191 (1997)

197. M Whittle, E Dickinson *J. Chem. Soc., Faraday Trans.* **94** 2453 (1998)
198. A H L West, J R Melrose, R C Ball *Phys. Rev. E* **49** 4237 (1994)
199. R Botet, P Rannou, M Cabane *Appl. Opt.* **36** 8791 (1997)
200. S Lambert, A Thill, P Ginestet, J M Audic, J Y Bottero *J. Colloid Interface Sci.* **228** 379 (2000)
201. A Thill, S Lambert, S Moustier, P Ginestet, J M Audic, J Y Bottero *J. Colloid Interface Sci.* **228** 386 (2000)
202. V M Shalaev, M I Shtokman *Zh. Eksp. Teor. Fiz.* **92** 509 (1987) [c]
203. S V Karpov, A K Popov, V V Slabko *Pis'ma Zh. Eksp. Teor. Fiz.* **66** 97 (1997) [f]
204. S V Karpov, A K Popov, V V Slabko, G B Shevnina *Kolloidn. Zh.* **57** 199 (1995) [b]
205. S V Karpov, A L Bas'ko, S V Koshelev, A K Popov, V V Slabko *Kolloidn. Zh.* **59** 765 (1997) [b]
206. S V Karpov, A L Bas'ko, A K Popov, V V Slabko *Kolloidn. Zh.* **62** 773 (2000) [b]
207. M Moskowits *Rev. Mod. Phys.* **57** 785 (1985)
208. A V Butenko, V M Shalaev, M I Shtokman *Zh. Eksp. Teor. Fiz.* **94** 107 (1988) [c]
209. V M Shalaev, R Botet *Phys. Rev. B* **50** 12987 (1994)
210. V A Markel', L S Muratov, M I Shtokman *Zh. Eksp. Teor. Fiz.* **98** 819 (1990) [c]
211. K Ghosh, R Fuchs *Phys. Rev. B* **38** 5222 (1988)
212. K Ghosh, R Fuchs *Phys. Rev. B* **44** 7330 (1991)
213. I H H Zabel, D Stroud *Phys. Rev. B* **46** 8132 (1992)
214. V M Shalaev, R Botet, V Butenko *Phys. Rev. B* **48** 6662 (1993)
215. V M Shalaev, R Botet, R Jullien *Phys. Rev. B* **44** 12216 (1991)
216. V M Shalaev, M I Stockman, R Botet *Physica A* **185** 181 (1992)
217. V M Shalaev, M Moskovits, A A Golubentsev, S John *Physica A* **191** 352 (1992)
218. V M Shalaev, V A Markel, V P Safonov *Fractals* **2** 201 (1994)
219. V M Shalaev, E Y Polyakov, V A Markel, R Botet *Physica A* **241** 249 (1997)
220. V M Shalaev, E Y Poakov, V A Markel *Phys. Rev. B* **53** 2437 (1996)
221. V A Markel, V M Shalaev, E B Stechel, W Kim, R L Armstrong *Phys. Rev. B* **53** 2425 (1996)
222. V V Maksimenko, A A Lushnikov *Pis'ma Zh. Eksp. Teor. Fiz.* **57** 204 (1993) [f]
223. V M Shalaev *Phys. Rep.* **272** 61 (1996)
224. S G Rautian, V P Safonov, P A Chubakov, V M Shalaev, M I Shtokman *Pis'ma Zh. Eksp. Teor. Fiz.* **47** 243 (1988) [f]
225. A V Butenko, P A Chubakov, Yu E Danilova, S V Karpov, A K Popov, S G Rautian, V P Safonov, V V Slabko, V M Shalaev, M I Stockman *Z. Phys. D: At., Mol. Clusters* **17** 283 (1990)
226. S V Karpov, A K Popov, S G Rautian *Pis'ma Zh. Eksp. Teor. Fiz.* **48** 528 (1988) [f]
227. M I Stokman, L N Pandey, L S Muratov, T F Gorge *Phys. Rev. Lett.* **72** 2486 (1994)
228. M I Stokman, L N Pandey, T F Gorge *Phys. Rev. B* **53** 2183 (1996)
229. M I Stokman *Phys. Rev. Lett.* **79** 4562 (1997)
230. M I Stokman *Phys. Rev. E* **56** 6494 (1997)
231. D P Tsai, J Kovacs, Z Wang, M Moskovits, V M Shalaev, J Sush, R Botet *Phys. Rev. Lett.* **72** 4149 (1994)
232. V M Shalaev, M Moskovits *Phys. Rev. Lett.* **75** 2451 (1995)
233. V A Markel, V M Shalaev, P Zhang, W Huynh, L Tay, T L Haslett, M Moskovits. *Phys. Rev. Lett.* **59** 10 903 (1999)
234. Yu E Danilova, S G Rautian, V P Safonov, P A Chubakov, V M Shalaev, M I Shtokman *Pis'ma Zh. Eksp. Teor. Fiz.* **47** 200 (1988) [f]
235. Yu E Danilova, S G Rautian, V P Safonov, P A Chubakov, V M Shalaev, M I Shtokman *Izv. Akad. Nauk, Ser. Fiz.* **60** 374 (1996)
236. V P Drachev, S V Perminov, S G Rautian, V P Safonov *Pis'ma Zh. Eksp. Teor. Fiz.* **68** 618 (1998) [f]
237. S Alexander, R Orbach *J. Phys. Lett (Paris)* **43** L625 (1982)
238. R Rammal, G Toulouse *J. Phys. Lett. (Paris)* **44** L13 (1983)
239. B Sapoval, Th Gobron, A Margolina *Phys. Rev. Lett.* **67** 2974 (1991)
240. A Bunde, H E Roman, S Russ, A Abroni, A B Harris *Phys. Rev. Lett.* **69** 3189 (1992)
241. A Petri, L Pietronero *Phys. Rev. B* **45** 12864 (1992)
242. V V Maksimenko *Opt. Atmosf. Okeana* **10** 21 (1997)
243. V V Maksimenko, V A Krikunov, A A Lushnikov *Zh. Eksp. Teor. Fiz.* **102** 1571 (1992) [c]
244. A K Sarychev, V M Shalaev *Phys. Rep.* **335** 275 (2000)
245. R D Hazlett *J. Colloid Interface Sci.* **137** 527 (1990)
246. S Shibuichi, T Onda, N Satoh, K Tsujii *J. Chem. Phys.* **100** 19512 (1996)
247. K Tsujii, T Yamamoto, T Onda, S Shibuichi *Angew. Chem., Int. Ed. Engl.* **36** 1011 (1997)
248. S Shibuichi *J. Soc. Powder Technol. Jpn.* **37** 260 (2000)
249. S Shibuichi,T Yamamoto, T Onda, K Tsujii *J. Colloid Interface Sci.* **208** 287 (1998)
250. V I Roldughin, N A Tikhonov *Dokl. Akad. Nauk* **383** 362 (2002) [g]
251. V V Maksimenko, A P Korobko, G B Andreev *Zh. Fiz. Khim.* **72** 1720 (1998) [a]
252. V V Maksimenko, A P Korobko, G B Andreev *Poverkhnost* (4) 40 (2001)
253. C D Tsakiroglou, A C Payatakes *Adv. Colloid Interface Sci.* **75** 215 (1998)
254. V D Borman, A M Grekhov, V I Troyan *Zh. Eksp. Teor. Fiz.* **118** 193 (2000) [c]
255. A V Neimark *Pis'ma Zh. Eksp. Teor. Fiz.* **51** 535 (1990) [f]
256. W I Friesen, R J Mikula *J. Colloid Interface Sci.* **120** 263 (1987)
257. B Zhang, S Li *Ind. Eng. Chem. Res.* **34** 1383 (1995)
258. B Sahouli, S Blacher, R Pirard, F Brouers *J. Colloid Interface Sci.* **214** 450 (1999)
259. B Zhang, S Li *Ind. Eng. Chem. Res.* **36** 1598 (1997)
260. C-K Lee *Ind. Eng. Chem Res.* **37** 3939 (1998)
261. J Hallet, J G Hudson, C F Rogers *Aerosol Sci. Technol.* **10** 70 (1989)
262. I Clobeck, L Appleby, E J Hardman, R M Harrison *J. Aerosol Sci.* **21** 527 (1990)
263. P-F Huang, B J Turpin, M J Pipho, D B Kittelson, P H McMurry *J. Aerosol Sci.* **25** 447 (1994)
264. E F Mikhailov, S S Vlasenko, A A Kiselev, T I Ryshkevich *Kolloidn. Zh.* **59** 195 (1997) [b]
265. A Schmidt-Ott *J. Aerosol Sci.* **19** 553 (1988)
266. A Schmidt-Ott *Appl. Phys. Lett.* **52** 954 (1988)
267. A J Hurd, W L Flower *J. Colloid Interface Sci.* **122** 178 (1988)
268. G Yang, P Biswas *Aerosol Sci. Technol.* **27** 507 (1997)
269. S N Rogak, R Flagan *Aerosol Sci. Technol.* **18** 25 (1993)
270. M K Akhtar, G G Lipscomb, S E Pratsinis *Aerosol Sci. Technol.* **21** 82 (1994)
271. R Sempere, D Bourett, T Woignier, J Phalippou, R Jullien *Phys. Rev. Lett.* **71** 3307 (1993)
272. D W Schaefer, B J Olivier, C Ashley, G Beaucage, D Richter, B Farago, B Frick, D A Fischer *J. Non-Cryst. Solids* **172/173** 393 (1994)
273. N Olivi-Tran, R Jullien, G W Cohen-Solal *Europhys. Lett.* **30** 393 (1995)
274. N Olivi-Tran, R Jullien *Phys. Rev. B* **52** 258 (1995)
275. N Olivi-Tran, R Jullien *J. Sol-Gel Sci. Technol.* **8** 813 (1997)
276. G Yang, P Biswas *J. Colloid Interface Sci.* **211** 142 (1999)
277. Z Deng, Y Liang, C Liu *J. Colloid Interface Sci.* **173** 79 (1995)
278. R Thouy, N Olivi-Tran, R Jullien *Phys. Rev. B* **56** 5321 (1997)
279. R Thouy, R Jullien *J. Phys. A* **9** 2953 (1994)
280. T C Vaimakis, C S Skordilis, P J Pomonis *J. Colloid Interface Sci.* **172** 311 (1995)
281. D Avnir (Ed.) *The Fractal Approach to Heterogeneous Chemistry: Surface, Colloids, Polymers* (Chichester: Wiley, 1989)
282. D Avnir, D Farin, P Pfeifer *New J. Chem.* **16** 439 (1992)
283. J P Hulin *Adv. Colloid Interface Sci.* **49** 47 (1994)
284. F Romm *J. Colloid Interface Sci.* **213** 322 (1999)
285. F Romm *J. Colloid Interface Sci.* **232** 121 (2000)
286. J Rouquerol, D Avnir, C W Fairbridge, D H Everett, J H Haynes, N Pernicone, J D F Framsay, K S W Sing, K K Unger *Pure Appl. Chem.* **66** 1739 (1994)
287. H D Bale, P W Schmidt *Phys. Rev. Lett.* **53** 596 (1984)
288. G Porod *Kolloidn. Zh.* **124** 83 (1951)
289. G Porod *Kolloidn. Zh.* **125** 51 (1951)
290. R Kirste, G Porod *Kolloidn. Zh., Z. Polym.* **184** 1 (1962)
291. A Ch Mitropoulos, N K Kanellopoulos, K L Sefanopoulos, R K Heenan *J. Colloid Interface Sci.* **203** 229 (1998)

292. F Gottsleben, D Hesse *Hung. J. Ind. Chem.* **20** 121 (1992)
293. V M Gu'ko *Teor. Eksp. Khim.* **36** 1 (2000) [h]
294. P Pfeifer,Y J Wu, M W Cole, J Krim *Phys. Rev. Lett.* **62** 1997 (1989)
295. D Avnir, M Jaroniec *Langmuir* **5** 1431 (1989)
296. Y Yin *Langmuir* **7** 216 (1991)
297. M Kardar, J O Indeqeu *Europhys. Lett.* **12** 161 (1990)
298. I M Kismail, P Pfaeifer *Langmuir* **10** 1532 (1994)
299. Y Lefehvre, C Jolicoeur *Colloid Surf.* **63** 67 (1992)
300. Y Lefehvre, S Lacelle, C Jolicoeur *J. Mater. Res.* **7** 1888 (1992)
301. A P Terzyk, P A Gauden, G Rychlicki, R Wojsz *Colloids Surf. A* **152** 293 (1999)
302. A P Terzyk, P A Gauden, G Rychlicki, R Wojsz *Langmuir* **15** 285 (1999)
303. V M Gun'ko, F Villieras, R Leboda, M Marciniak, B Charmas, J Skubiszewska-Zieba *J. Colloid Interface Sci.* **230** 320 (2000)
304. A V Neimark, K K Unger *J. Colloid Interface Sci.* **158** 412 (1993)
305. A V Neimark, M Hanson, K K Unger *J. Phys. Chem.* **97** 6011 (1993)
306. S Lebon, R Hiller *J. Colloid Interface Sci.* **173** 215 (1995)
307. M Kolb *J. Non-Cryst. Solids* **121** 227 (1990)
308. F Meng, J R Schlup, L T Fan *J. Colloid Interface Sci.* **197** 88 (1998)
309. J Esquena, C Solans, J Llores *J. Colloid Interface Sci.* **225** 291 (2000)
310. M Jaroniec, M Kruk, J P Olivier *Surf. Sci.* **342** L1127 (1995)
311. J P Olivier *J. Porous Mater.* **2** 9 (1995)
312. M Jaroniec, M Kruk, J P Olivier *Langmuir* **13** 1031 (1997)
313. M Kardar, J O Indeqeu *Phys. Rev. Lett.* **65** 662 (1990)
314. T Voung, P A Monson *Langmuir* **12** 5425 (1996)
315. J Dachs, S J Eisenreich *Langmuir* **15** 8686 (1999)
316. J M Williams, T P Beebe *J. Phys. Chem.* **97** 6249 (1993)
317. A V Neimark *Phys. Rev. B* **50** 15435 (1994)
318. J J Wu *Chaos, Solitons, Fractals* **12** 2481 (2001)
319. J J Wu *Chaos, Solitons, Fractals* **13** 1791 (2002)
320. Ya L Kobelev, L Ya Kobelev, E P Romanov *Dokl. Akad. Nauk* **370** 757 (2000) [g]
321. S I Bozhevolnui, B Vohsen, A Zayats, I I Smolyaninov *Surf. Sci.* **356** 268 (1996)
322. M S Mattsson, G A Niklasson, C G Granqvist *Phys. Rev. B* **54** 17884 (1996)
323. A Provata, P Falaras, A Xagas *Chem. Phys. Lett.* **297** 484 (1998)
324. A T Yinnon, D A Lidar (Hamburger), I Farbman, R B Gerber, P Zeppenfeld, M A Krzyzowski, G Cosma *J. Chem. Phys.* **106** 4228 (1997)
325. C Houng-Van, B Pommier, R Harivololona, P Pichat *J. Non-Cryst. Solids* **145** 250 (1992)
326. J Livage, M Henry, C Sanchez *Prog. Solid State Chem.* **18** 259 (1988)
327. S Henning, L Svensson *Phys. Scr.* **23** 697 (1981)
328. R Caps, J Fricke *Sol. Energy* **36** 361 (1986)
329. W Cao, J Hunt *Appl. Phys. Lett.* **64** 2376 (1994)
330. S B Xiong, Z M Ye, Z G Liu, W P Ding, X Q Zheng, Y P Zhu, C Y Lin *Mater. Lett.* **32** 165 (1997)
331. G W Scherer *Adv. Colloid Interface Sci.* **76–77** 321 (1998)
332. T Lours, J Zarzycki, A Graievich, D I Dos Santos, M Aegerter *J. Non-Cryst. Solids* **95–96** 1151 (1987)
333. A Yasumori, H Kawazoe, M Yamane *J. Non-Cryst. Solids* **100** 215 (1988)
334. R Vacher, T Woignier, J Pelows, E Courtens *Phys. Rev. B* **37** 6500 (1988)
335. F Chaput, J P Boilot, A Dauger, F Devreux, A de Geyer *J. Non-Cryst. Solids* **116** 133 (1990)
336. R Vacher, E Couertens, E Scoll, M Böffgen, H Rothuizen *J. Phys.: Condens. Matter* **3** 6531 (1991)
337. R F Reidy, A J Allen, S Krueger *J. Non-Cryst. Solids* **285** 181 (2001)
338. A J Allen, S Krueger, G Skandan , G G Long, H Hahn, H M Kerch, J C Parker, M N Ali *J. Am. Ceram. Soc.* **79** 1201 (1996)
339. G G Long, S Krueger, P R Jemian, D R Black, H E Burdette, J P Cline, R A Gerhardt *J. Appl. Crystallogr.* **23** 535 (1990)
340. T Woignier, J Reynes, J Phalippou, J L Dussossoy *J. Sol-Gel Sci. Technol.* **19** 835 (2000)
341. C Marliere, T Woignier, P Dieudonne, J Primera, M Lamy, J Phalippou *J. Non-Cryst. Solids* **295** 175 (2001)
342. B Knoblich, Th Gerber *J. Non-Cryst. Solids* **296** 81 (2001)
343. J Gun, O Lev, O Regev, S Pevzner, A Kucernak *J. Sol-Gel Technol.* **13** 189 (1998)
344. A Emmerling, J Fricke *J. Sol-Gel Sci. Technol.* **8** 781 (1997)
345. G W Scherer, D M Smith, X Qiu, J M Anderson *J. Non-Cryst. Solids* **186** 316 (1995)
346. R Pirard, J-P Pirard *J. Non-Cryst. Solids* **212** 262 (1997)
347. R Calemczuk, A M de Goer, B Salce, R Maynard, A A Zarembowitch *Europhys. Lett.* **3** 1205 (1987)
348. E Courtens *J. Phys. IV* **2** 3 (1992)
349. T Terao, A Yamaya, T Nakayama *Phys. Rev. E* **57** 4426 (1998)
350. E Courtens, J Pelous, J Phalippou, R Vacher, T Woignier *Phys. Rev. Lett.* **58** 128 (1987)
351. R Maynard *Physica A* **157** 601 (1989)
352. S Alexander, E Courtens, R Vacher *Physica A* **195** 286 (1993)
353. E Anglaret, I Beurroies, L Duffours, C Levelut, M Foret, P Delord, T Woignier, J Phalippou, J Pelous *J. Non-Cryst. Solids* **225** 248 (1998)
354. C Levelut, E Anglaret, J Pelous *J. Non-Cryst. Solids* **225** 272 (1998)
355. I Beurroies, L Duffours, P Delord, T Woignier, J Phalippou *J. Non-Cryst. Solids* **241** 38 (1998)
356. T Woignier, J Reynes, A Hafidi Alaoui, I Beurroies, J Phalippou *J. Non-Cryst. Solids* **241** 45 (1998)
357. W L Huang, K M Liang, S R Gu, S H Cui *J. Mater. Sci. Lett.* **19** 1681 (2000)
358. S Roy, R Dasgupta, S Tarafdar *Solid State Ionics* **86–88** 383 (1996)
359. C Marliere, F Despetis, P Etienne, T Woignier, P Dieudonne, J Phalippou *J. Non-Cryst. Solids* **285** 148 (2001)
360. A Hasmy, M Foret, E Anglaret, J Pelous, R Vacher, R Jullien *J. Non-Cryst. Solids* **186** 118 (1995)
361. R Jullien, N Olivi-Tran, A Hasmy, T Voignier, J Phalippou, D Bourret, R Sempere *J. Non-Cryst. Solids* **188** 1 (1995)
362. A Hasmy, N Olivi-Tran, R Jullien *J. Phys.: Condens. Matter* **10** 4947 (1998)
363. I Beurroies, D Bourret, R Sempere, J Phalippou *J. Non-Cryst. Solids* **186** 328 (1995)
364. F Meng, J R Schlup, L T Fan *Chem. Mater.* **9** 2459 (1997)
365. C K Lee, C S Tsay *J. Phys. Chem. B* **102** 4123 (1998)
366. A B Jarzebski, J Lorenc, L Pajak *Langmuir* **13** 1280 (1997)
367. W L Huang, K M Liang, S H Cui, S R Gu *J. Colloid Interface Sci.* **231** 152 (2000)
368. C-S Tsay, C-K Lee, A S T Chiang *Chem. Phys. Lett.* **278** 83 (1997)
369. M-A Einarsrud, M B Kirkedelen, E Nilsen, K Mortensen, J Samseth *J. Non-Cryst. Solids* **231** 10 (1998)
370. L I Kheifets, Yu V Pavlov, P V Krylenko *Izv. Akad. Nauk, Ser. Khim.* 781 (2000) [i]
371. Yu V Pakharukov, T E Shevnina *Pis'ma Zh. Eksp. Teor. Fiz.* **69** 900 (1999) [f]
372. Yu V Pakharukov, T E Shevnina *Pis'ma Zh. Tekhn. Fiz.* **27** 85 (2001) [d]
373. J Milum, A Sadana *J. Colloid Interface Sci.* **187** 128 (1997)
374. A Sadana *J. Colloid Interface Sci.* **190** 232 (1997)
375. A Sadana *J. Colloid Interface Sci.* **198** 164 (1999)
376. A Ramakrishnan, A Sadana *J. Colloid Interface Sci.* **213** 465 (1999)
377. A Ramakrishnan, A Sadana *J. Colloid Interface Sci.* **229** 628 (2000)
378. A Sadana, A Ramakrishnan *J. Colloid Interface Sci.* **234** 9 (2001)
379. B J West, D R Bickel *Physica A* **249** 544 (1998)
380. T Lahiri, N S Kar, A Chakrabarti, A K Dasgupta *J. Colloid Interface Sci.* **211** 89 (1999)
381. D Risovic, M Martinis *J. Colloid Interface Sci.* **182** 199 (1996)
382. D Risovic *J. Colloid Interface Sci.* **197** 391 (1998)
383. A H Tompson *Annu. Rev. Earth Planet. Sci.* **19** 237 (1991)
384. A P Radlinski, E Z Radlinska, M M Agamalian, G D Wignall, P Linder, O W Randl *Phys. Rev. Lett.* **82** 3078 (1999)
385. A P Radlinski, E Z Radlinska, M M Agamalian, G D Wignall, P Linder, O W Randl *J. Appl. Crystallogr.* **33** 860 (2000)
386. P Meakin *Science* **252** 226 (1991)

387. G V Vstovskii *Zh. Prikl. Mekh. Tekhn. Fiz.* 130 (1992)
388. I Zh Bunin, G V Vstovskii *Izv. Akad. Nauk, Metally* 29 (1992)
389. V Silberschmidt *J. Phys. IV* **6** 287 (1996)
390. G V Vstovskii, I Zh Bunin, A G Kolmakov, I Yu Tanitovskii *Dokl. Akad. Nauk* **343** 613 (1995) [g]
391. K Hisatsune, Y Takuma, Y Tanaka, K Udoh , K Kawasaki *J. Mater. Sci.* **33** 4783 (1998)
392. M Tanaka, A Kayama, Y Ito, R Kato. *J. Mater. Sci.* **33** 5747 (1998)
393. L A Dovbnya, D E Naumov, B V Khramov *Pis'ma Zh. Eksp. Teor. Fiz.* **73** 410 (2001) [f]
394. Y C Guilaume, E Peyrin, C Guinchard *J. Phys. Chem. B* **103** 5608 (1999)
395. D Xie, J Wu, G Xu, Q Ouyang, R D Soloway, T Hu *J. Phys. Chem. B* **103** 8602 (1999)

[a] — *Russ. J. Phys. Chem. (Engl. Transl.)*
[b] — *Colloid J. (Engl. Transl.)*
[c] — *J. Exp. Theor. Phys. (Engl. Transl.)*
[d] — *Techn. Phys. Lett. (Engl. Transl.)*
[e] — *Chem. Phys. Rep. (Engl. Transl.)*
[f] — *J. Exp. Theor. Phys. Lett. (Engl. Transl.)*
[g] — *Dokl. Chem. (Engl. Transl.)*
[h] — *Theor. Exp. Chem. (Engl. Transl.)*
[i] — *Russ. Chem. Bull., Int. Ed. (Engl. Transl.)*